



**HAL**  
open science

## Reaction dynamics within a cluster environment

Marc Briant, Jean-Michel Mestdagh, Marc-André Gaveau, Lionel Poisson

► **To cite this version:**

Marc Briant, Jean-Michel Mestdagh, Marc-André Gaveau, Lionel Poisson. Reaction dynamics within a cluster environment. *Physical Chemistry Chemical Physics*, 2022, 10.1039/D1CP05783A . cea-03633216

**HAL Id: cea-03633216**

**<https://cea.hal.science/cea-03633216>**

Submitted on 6 Apr 2022

**HAL** is a multi-disciplinary open access archive for the deposit and dissemination of scientific research documents, whether they are published or not. The documents may come from teaching and research institutions in France or abroad, or from public or private research centers.

L'archive ouverte pluridisciplinaire **HAL**, est destinée au dépôt et à la diffusion de documents scientifiques de niveau recherche, publiés ou non, émanant des établissements d'enseignement et de recherche français ou étrangers, des laboratoires publics ou privés.

# Reaction Dynamics within a Cluster Environment

Marc Briant,<sup>a</sup> Jean-Michel Mestdagh,<sup>a</sup> Marc-André Gaveau,<sup>a</sup> and Lionel Poisson<sup>\*b</sup>

This perspective article reviews experimental and theoretical works where rare gas clusters and helium nanodroplet are used as nanoreactor to investigate chemical dynamics in a solvent environment. A historical perspective is presented first, then specific considerations on the mobility of reactants within these reaction media. The dynamical response of pure clusters and nanodroplets to photoexcitation is shortly reviewed before examining the role of the cluster (or nanodroplet) degrees of freedom on the photodynamics of the guest atoms and molecules.

## 1 Introduction

Reaction dynamics is a branch of physical chemistry which interrogates conceptually, theoretically, computationally and experimentally the force field that drives elementary processes as electron transfer, structural deformation, bond rearrangement and so on. A common feature in these processes is that structure, dynamics and chemical function are interrelated. They are at play in a variety of environments, ranging from isolated molecules to clusters, nanoscale objects, macroscopic condensed phases and biological environments. A short, nevertheless comprehensive history of the field was drawn fifteen years ago by Jortner together with considerations on the laser control of chemical reactions.<sup>1</sup> The history dates back to almost 100 years, when Bonhoeffer and Farkas used the uncertainty principle by Heisenberg to relate the diffuse character of molecular spectra to the lifetime of the states that are excited, hence establishing that spectroscopic observations can bring dynamical informations on the photodissociation processes that control the lifetime of these states.<sup>2</sup> This paved the way for developing concepts that help modeling intramolecular and intermolecular processes within isolated species, clusters and condensed phases, within biophysical/biochemical environments and most recently to treat of electron dynamics. The book "Molecular Reaction Dynamics" authored by Levine is an extensive overview of these research fields, about 15 years ago<sup>3</sup>.

Beyond their intrinsic significance in physical chemistry, atomic and molecular clusters play an important role in many scientific areas. Referring to atmospheric sciences, Elm *et al.* pointed out in 2020 that "[...] the scientific interest in atmospheric molecular clusters has steadily increased and [...] presents a relatively new and rapidly expanding field of research".<sup>4</sup> More recently Smith *et al.* illustrated the central role of these clusters in the growth of atmospheric aerosols and consequently as link between atmospheric chemistry and climate.<sup>5</sup> Experiments where molecules are deposited on large clusters are extensively reviewed by Fárník *et al.* from a physical chemist point of view, with special focus on processes that are relevant to atmospheric and interstellar chemistry.<sup>6</sup> Many more examples of this type could be given outside the context of earth sciences.

Because of their double nature (tools to develop fundamen-

tal concepts in physical chemistry and objects with applications in many research areas) atomic and molecular clusters received a continuous attention since the early 1980's from those people involved in reaction dynamics. Works prior to approximately 2000 are overviewed in the two volume book "Clusters of Atoms and Molecules I and II" edited by Haberland,<sup>7,8</sup> and in a book by Johnston.<sup>9</sup> A series of review papers highlight the subject also.<sup>10-14</sup> Finally, the experimental techniques used to generate clusters and properties of van der Waals clusters are extensively reviewed by Bostedt *et al.* in Ref. 15.

Basic concepts behind this activity are extensively developed in the proceedings of the 1988 "Enrico Fermi" International School of Physics,<sup>16</sup>. Often, clusters are considered as providing a link between the macroscopic and the microscopic approaches of physical sciences, which are otherwise unconnected. This appears strikingly in a series of review papers by Jortner,<sup>17,18</sup>, Bartell,<sup>14</sup> Hartke,<sup>19</sup> and Berry and Smirnov.<sup>20</sup> The connection between cluster physical chemistry and the exploding field of nanosciences is emphasized in a review paper by Baletto and Ferrando.<sup>21</sup>

When focusing specifically on reaction dynamics, clusters have attracted attention very early as tools for unraveling solvation effects. Microsolvation which focuses attention on solute/solvent intermolecular interactions must be distinguished from macrosolvation where global properties of the solvent are considered.<sup>22</sup> Cluster models where solvation shells are constructed gradually around solute molecules are relevant of microsolvation. Works by Leutwyler and Bosiger<sup>23,24</sup> and by M. Mons and coworkers<sup>25</sup> furnish early examples in this direction. However, Truhlar and coworkers suggested that the microsolvation cluster model might not be fully adequate to mimic solvation in a bulk liquid. A test example was the activation free energy for decarboxylation of 4-pyridylacetic acid zwitterion in water. A discrete cluster model with two water molecules, a continuum description of water, and a mixed discrete-continuum model furnished significantly different values of the activation energy. It is not clear however which one is most realistic.<sup>26</sup> The microsolvation/macrosolvation issue has been re-examined very recently by considering UV-visible and IR spectra of a solvatochromic pyridinium-N-phenolate dye in various solvation environments (rare gas matrices; mixtures of argon and water; water ice).<sup>27</sup> The present perspective includes considerations on microsolvation but the central point of view is different, large clusters being considered as reaction media rather than as building blocks.

Limiting our attention to reaction dynamics within rare gas

<sup>a</sup>Université Paris-Saclay, CEA, CNRS, LIDYL, 91191, Gif-sur-Yvette, France.

<sup>b</sup>Université Paris-Saclay, CNRS, Institut des Sciences Moléculaires d'Orsay, 91405, Orsay, France.

\* E-mail:lionel.poisson@universite-paris-saclay.fr

clusters, a distinction must be drawn between helium nanodroplets which are quantum in nature and clusters of heavier rare gases, which do not have this character. Our research group performed reaction dynamics studies in both environments. Yet unpublished experimental and theoretical works of our laboratory are presented here and are put in perspective with works of the literature. This focus meets that of recent perspective articles in PCCP (Refs. 6,28–30) and a review communication by Mudrich *et al.*<sup>31</sup> The perspective article by Fárník *et al.*<sup>6</sup> deals with species embedded in heavy rare gases, chosen for their relevance in environmental and astrophysical physical chemistry, that of Hochlaf<sup>28</sup> primarily focuses on theoretical approaches, that of Ahmed and Kostko<sup>29</sup> on systems that can be studied by synchrotron radiation, that of Ernst and Hauser<sup>30</sup> on metal clusters embedded in helium nanodroplets and the review by Mudrich *et al.*<sup>31</sup> deals with the response of helium nanodroplets to electronic excitation.

The present perspective article starts with a brief history of using clusters as nanoreactor to investigate chemical dynamics in a solvent environment (Sec. 2). A few words are added to present the pick-up technique, which is at the centre of these studies (Sec. 3). The mobility of reactants at the surface of heavy rare gas clusters and within helium nanodroplet is evoked in Sec. 4. Then, reaction dynamics studies within clusters are reviewed. Photoexcitation is often present in the reported works and we may wonder about its effect on the cluster (or nanodroplet) itself. We thus start presenting the dynamical response of pure clusters and nanodroplets to photoexcitation (Sec. 5) before examining to which extent and by which mechanisms, cluster (or nanodroplet) degrees of freedom affect the photodynamics of a single guest atom (Sec. 6) as the unimolecular (Sec. 7), bimolecular (Sec. 8) and multimolecular (Sec. 9) photodynamics of guest molecules. Perspectives are drawn in Sec. 10, which complement those already present in the previous sections.

## 2 Rare gas clusters as chemical nanoreactor, a historical perspective

The use of clusters to study chemical reactions in a solvated environment has been introduced by E.R. Bernstein and coworkers more than thirty years ago.<sup>32</sup> The idea was to carry reactant and solvent molecules in a supersonic beam of helium to generate clusters where a single reactant molecule is associated with a few solvent molecules. The reaction was interrogated through laser induced fluorescence, dispersed emission, or through the coupling between time-of-flight mass spectroscopy and resonance enhanced two photon ionization.<sup>33</sup> Many reactions were explored, including solvent-induced electron-transfer reactions, excited-state proton transfer in neutral clusters (explored by time resolve pump-probe experiments in the picosecond regime), cluster ion and radical chemistry.<sup>32</sup>

That clusters could act as a reaction medium of finite size has been proposed theoretically at about the same time by Kaukonen *et al.* who performed molecular dynamics calculations to model collisions between reactants embedded in rare gas clusters.<sup>34</sup> The concept was demonstrated for the  $\text{Na}_4\text{Cl}_3^+(\text{Ar})_{12,32} + \text{Cl}^-$  and

$\text{Na}_{14}\text{Cl}_{12}^{2+}(\text{Ar})_{30} + \text{Cl}^-$  reactions. The calculations showed that clusters was acting as a heat reservoirs to promote reactions.

The pick-up technique developed by Scoles and coworkers,<sup>35</sup> *i.e.* the collisional deposition of reactants on clusters in a cluster beam, allowed Lallement *et al.* using large argon clusters as nanoreactors.<sup>36</sup> Argon clusters carrying 200 to 1000 atoms were generated in a supersonic expansion of pure argon; a  $\text{N}_2\text{O}$  molecule was deposited at their surface and the resulting beam carrying  $\text{N}_2\text{O}(\text{Ar})_n$  clusters was crossed with a barium beam. The chemiluminescent  $\text{Ba} + \text{N}_2\text{O}$  forming electronically excited  $\text{BaO}$  was observed. Although this was not understood immediately, this experiment translated the prediction of Kaukonen *et al.* into what will be called later the Cluster Isolated Chemical Reaction (CICR) technique.<sup>37</sup> Two reactants, Ba and  $\text{N}_2\text{O}$  deposited on the same argon cluster have enough mobility within the cluster to collide each other and react.

The CICR technique deals with clusters of heavy rare gases (neon, argon, etc.). Independently, Scoles and coworkers developed the Helium NanoDroplet Isolation (HENDI) technique where the reactants are deposited on helium nanodroplets.<sup>38,39</sup> The latter are extremely cold (0.38 K)<sup>40</sup> and superfluid.<sup>41</sup> An early history of the field reviewed by Toennies and Vilesov where isolation in helium droplet was compared to isolation in bulk liquid helium.<sup>42</sup> The initial idea of HENDI experiments was to perform infrared absorption spectroscopy measurements of a single reactant molecule, taking advantage of the extreme fragility of the helium nanodroplets. The latter evaporate indeed when an infrared laser is tuned to a vibrational transition of the guest molecule. Recording the depletion of helium nanodroplets in the beam while scanning the infrared laser, directly documents the absorption spectrum of the guest molecule. Then, the technique evolved toward picking-up several reactants and, using the laser induced fluorescence detection technique, spectroscopic information could be obtained on the excited state spectroscopy of alkali dimers with ro-vibrational resolution.<sup>43–46</sup> With these studies, helium nanodroplets could be considered as ultracold nanomatrices where molecular complexes are formed and reacted.<sup>47</sup>

A parallelism can be drawn between CICR and HENDI reaction dynamics studies. For example, the  $\text{Ba} + \text{N}_2\text{O}$  reaction which is mentioned above to illustrate the power of CICR experiments has also been studied in a HENDI experiment.<sup>48</sup> In both experiments, the reaction proceed at the cluster/droplet surface and the same two reaction channels are observed, whether the electronically excited  $\text{BaO}$  product is vibrationally hot or cold. The HENDI experiment offers the additional possibility, when adding several xenon atom to the helium nanodroplet, to move the  $\text{Ba} + \text{N}_2\text{O}$  reaction inside the nanodroplet. The channel forming cold  $\text{BaO}^*$  is then almost exclusive.<sup>48</sup>

For closing this historical section, we recall a proposition formulated in the group of R.D. Levine on the ground of molecular dynamics calculations. It takes advantage that a cluster carrying molecular oxygen and nitrogen molecules is enough over-heated by supersonic impact on a surface that the “air burning” reaction  $\text{N}_2 + \text{O}_2 \longrightarrow 2\text{NO}$  is turned on.<sup>49</sup> This very original use of a cluster as “hot reaction cell” received no direct experimental evidence yet. Ceyer and coworkers introduced the related concept of

“Chemistry with a hammer” under which, dissociative chemisorption of CH<sub>4</sub> molecules adsorbed by Ni(111) surfaces was stimulated by impact of Ar atoms on the Nickel surface.<sup>50</sup> This concept still retains computational attention.<sup>51</sup>

### 3 The pick-up, a dedicated technique to add reactants to clusters and nanodroplets

Most of the experiments reported in this perspective use the pick-up technique for adding reactants (atoms or molecules) to free clusters or nanodroplets. This elegant and versatile method has been introduced by Scoles and coworkers in the 1980’s.<sup>35</sup> The key idea is to pass a beam carrying clusters (or nanodroplets) through a cell (the pick-up cell) filled with a vapor of the reactant(s) to be deposited. Along their path through the cell, the clusters make sticky collisions with reactant particles. This forms a new species where one or several reactant particles are attached to the cluster, a way to isolate these particles within a controlled environment of finite size. In a sense, this mirrors within a reaction medium, the technique introduced by Jovet and Soep where two reactants, which are bound to each other in a 1:1 van der Waals complex, are isolated in a supersonic beam.<sup>52</sup>

The sticky character of the collision between clusters of heavy rare gases (neon, argon, etc) and a buffer gas has been modeled a long time ago in molecular dynamics calculations.<sup>53-55</sup> A motivation was to establish numerically under which circumstances such a cluster acts as a sufficiently good heat sink to absorb the collision energy and capture the reactants. An alternative motivation was to decide whether the reactants that are picked-up are located at the surface or in the volume of the cluster.

This issue has been examined experimentally a few years ago when depositing metal atoms (K and Ba) on argon clusters.<sup>56,57</sup> Very efficient pick-up was found with barium whereas the contrary was observed with potassium. This difference reflects the deeper Ba-Ar interaction energy (95 cm<sup>-1</sup> for Ba-Ar<sup>58</sup> versus 59 cm<sup>-1</sup> for K-Ar<sup>59</sup>) associated with an extremely favourable Ba/Ar mass ratio which drives barium into the cluster and relaxes efficiently the excess pick-up energy.

Three aspects of the pick-up technique are interesting to consider quantitatively: (i) the energy deposited by the sticky collisions; (ii) the pick-up cross-section and (iii) the number of reactant carried by the clusters. Apparently, no much ambiguity exists with these issues. First, the relative collision energy between the cluster and the guest summed with the cluster/guest binding energy is absorbed by the cluster/droplet as internal heat upon a sticky collision. Second, the pick-up probability is controlled by the geometrical cross-section of the cluster and third, it is a stochastic process with no memory between successive events. Hence, the number  $k$  of reactant picked up by the same cluster/droplet follows a Poisson statistics of order  $k$ :  $P_k(\langle n \rangle) = \frac{\langle n \rangle^k}{k!} \exp(-\langle n \rangle)$  where  $\langle n \rangle$ , the single parameter of Poisson distributions, is the average number of reactant particles deposited *per* cluster/droplet. This characteristics has been used to determine the stoichiometry of bimolecular reactions in CICR experiments.<sup>37</sup> Ideally, the reaction signal is monitored as a function of  $\langle n \rangle$  for each reactant. The Poisson distribution or

the linear combination of Poisson distributions which best fit the  $\langle n \rangle$  dependence of the reactive signal for each reactant indicates the exact stoichiometry of the reaction.

Unfortunately, this apparent simplicity bypasses important points:

- The velocity of both the clusters and the reactants may have broad distributions that affect their relative collision energy and therefore the amount of energy that is deposited by the pick-up process. Liang and Kresin derived an exact expression of the energy deposition when the reactant has a Maxwell-Boltzmann velocity distribution.<sup>60</sup>
- Energy is not the only conservation law in sticky collisions. Momentum and angular momentum conservation must be considered. Depending on the impact parameter, the collision energy is shared between internal energy (momentum conservation) and the rotational energy (angular momentum conservation). As a consequence, the amount of deposited energy can be broadly distributed. This aspect was investigated by Awali *et al.* for estimation of the rotational temperature of large argon clusters after sticky collisions with DABCO molecules (see Sec.7.2).<sup>61</sup>
- At slow relative velocities between the reactant and the cluster, attractive long-range forces affect the cross-section of sticky collisions and therefore affects the uptake of reactants on clusters. This effect is extensively reviewed in the perspective article by Fárník *et al.*<sup>6</sup> A theoretical work by Vigué *et al.* emphasizes the role of long range forces.<sup>62</sup> Analytic potentials<sup>63,64</sup> and a Langevin capture model were used to calculate the cross section of sticky collisions between an argon atom and an argon cluster of size  $n$ . The cross section was found to scale as  $n^{\frac{2}{3}}$  when  $n$  is smaller than  $\approx 1000$ . For larger values of  $n$ , the centrifugal barrier, which acts as capture radius in the Langevin model, moves closer to the cluster radius and the scaling law switches to geometric ( $n^{\frac{2}{3}}$ ).
- When several reactants are present on the same cluster/nanodroplet, they likely associate together. The additional energy term due to their binding energy has to be considered in the energy balance of the cluster/droplet. Note that incomplete association between reactants may be considered also.
- Internal energy is lost by the clusters (or droplets) when they evaporate partly after the pick-up. This also affects the subsequent pickup processes and the no memory assumption on which Poisson’s law is based may not be valid.

In relation with the last point, cross-section of sticky collisions, energy deposition and departure from the Poisson statistics are connected issues, especially when extremely fragile helium nanodroplets are considered. Stienkemeier and coworkers have examined this point very carefully with a special focus on the formation of alkali clusters within helium droplets.<sup>65,66</sup> Both numerical simulations and experimental observations in the latter

works reveal significant deviations from Poissonian distributions in droplets formed with several thousands of helium atoms, especially when 3 or more alkali atoms are picked-up.

Still considering the pick-up by helium nanodroplets, that of a rare gas atom has been modeled theoretically in a quantum description of the nanodroplet.<sup>67–69</sup> Subsequent formation of a rare gas dimer within the nanodroplet has been modelled also, both in full quantum and a hybrid quantum (helium)/classical (rare gas) approaches.<sup>70,71</sup> Helium density waves (possibly carrying vortices), which are produced by the pick-up of the Ne atoms, were shown to drive the Ne movements within the droplet and control their association as dimer. Similar calculations are also available for the pick-up of a Cs atom.<sup>72</sup> Again, a rich variety of dynamical phenomena were observed within the droplet, depending on the energy and angular momentum (*i.e.* impact parameter) of the impinging Cs atom.

Turning to the pick-up by heavy rare gases, Fedor *et al.* examined the cross-section of sticky collisions and the pick-up statistics in experiments where H<sub>2</sub>O, HBr, and CH<sub>3</sub>OH molecules are picked-up by free Ar<sub>*n*</sub> clusters.<sup>73</sup> The cluster slowdown due to the momentum transfer is used to monitor the pick-up efficiency. These experiments were complemented by Monte-Carlo and molecular dynamics simulations, assuming that the Ar-Ar and Ar-molecule interactions are described by a simple Lennard-Jones potential. As mentioned in several studies reported above, the cross-sections of sticky collisions can be larger than geometrical cross sections and the Poisson distribution method must be examined carefully when the number of picked up molecules is to be determined.

## 4 Reactant mobility within clusters/nanodroplets

It is almost tautological to say that observing bimolecular or multimolecular reactions in CICR or HENDI experiments implies that the reactants do not stay solvated independently within the cluster/droplet but move relative to one another, collide and eventually react when the transition state of the reaction has been crossed. In this context, mobility of the reactants in the cluster/droplet environment is a central concept. Of course, it appears differently in quantum helium nanodroplets (HENDI experiments) and in clusters of heavier rare gases (CICR experiments) which are not superfluid.

### 4.1 Association between reactants in helium droplets

The capture of several atomic or molecular species in helium nanodroplets is commonly admitted to form a complex with a similar structure as that observed in the gas phase. The large mobility within the superfluid nanodroplet, combined with the low nanodroplet temperature and finite size is believed to favor collisions, coalescence and eventually stabilization of complexes under their energetically most stable structure. Nevertheless, notable exceptions exist where dynamical effects prevent the most stable complexes to be formed. The group of Miller has been very active in this field. For example, long molecular chains are formed in helium nanodroplets by molecules which, as HCN, carry a

large electric dipole.<sup>74</sup> This was interpreted in a purely dynamical way, assuming that the cooling by the helium environment is so rapid that the condensing molecules stay trapped with the orientation geometry they have adopted immediately after the pick-up. Accordingly, each newly trapped HCN molecule is driven and trapped in a head-to-tail orientation with respect to the dipole created by the molecules that are already trapped. This favors the formation of linear chains. Similarly, a cyclic water hexamer is also observed although its energy is higher than that of the cage structure reported in the gas phase.<sup>75</sup> Another example is provided when aggregation between metal atoms and/or metal clusters is driven by quantum vortices within the thermodynamically stable state of a large superfluid helium nanodroplet. Such a situation is reported by the group of Vilesov who observed elongated Ag aggregates, which are believed to track internal movements of vortices.<sup>76</sup> This observation is currently turned into an elegant and versatile technique for producing a variety of wire-like metallic and possibly bimetallic aggregates.<sup>30</sup> The physics which controls quantum vortices, the emergence of vortices in rotating helium nanodroplets and the imaging of vortex structures are extensively reviewed by Gessner and Vilesov.<sup>77</sup>

### 4.2 Diffusion within clusters of heavy rare gases

The question of mobility appears differently in heavy rare gas clusters because of the non-quantum character of these clusters. It is an important issue since it fully controls reactions rates within clusters. We consider that it has not received enough attention in the literature, especially in the recent literature where this subject is almost absent. We hope to stimulate activity in this field with the review below. Fárník *et al.* in his 2021 perspective article make a similar observation. These authors consider molecular deposition on water clusters and write: "Theoretical investigations could elucidate the interplay of forces acting between the molecules on nanoparticles, which lead to their mobility and coagulation."<sup>6</sup>

Here we concentrate on clusters of heavy rare gases. Two points must be discussed first: the phase of the clusters (liquid or solid) and the location of the guest particles (interior *versus* surface of the cluster).

The coexistence between liquid and solid phases and between several solid phases in clusters of heavy rare gases is a very difficult and highly debated issue.<sup>20,78,79</sup> It relies a lot on which criterium is chosen to decide that a liquid phase is present in a medium of finite size. Such criteria may indeed be ill-defined in very small media (*e.g.* a few tens of atoms). Without entering the debate, let us note that in clusters carrying more than 50 atoms, the solid phase is stable enough and has a sufficiently large extension within the clusters to allow for electron diffraction studies.<sup>80–82</sup>

An immediate issue when adding reactants to clusters with a solid core is whether guest particles solvate in the interior of the solid phase or stay more or less embedded in the cluster surface. This was first answered theoretically by Perera and Amar who performed molecular dynamics calculations and showed that answer to this question is essentially provided by the binding energy

and the equilibrium distance between the reactant and a single constituent of the cluster<sup>83</sup>. With a long distance shallow well between these species, the reactant stays at the surface of the cluster. On the contrary, a deep well at short distance stimulate the formation of a solvation shell about the reactant, which therefore looks as migrating in the interior of the cluster. This was checked spectroscopically also and further documented theoretically by a pseudo-diatomic picture of the guest-cluster interaction when a single barium atom or a single calcium atom is added to a cluster of several hundreds of argon atoms.<sup>84,85</sup> The Ba-Ar<sup>58</sup> and Ca-Ar<sup>86</sup> interaction potentials have a shallow well at long distance and as expected, surface solvation was observed in both cases.

Beyond these studies, the migration and mobility of reactants within large clusters of heavy rare gases has attracted only few and very old studies either experimentally,<sup>87-89</sup> or theoretically.<sup>55</sup> Experimentally, a barium atom was added to a large argon cluster, it was laser excited to the  $6s6p^1P$  level and the fluorescence emission  $6s6p^1P \rightarrow 6s^2^1S$  was recorded. Then, Lallement *et al.* added methane molecules to the cluster and observed that the fluorescence signal is quenched, indicating that when a Ba atom and one or several CH<sub>4</sub> are present on the same cluster they move relative to each other and make a quenching collision. If the timescale of such movement is much larger than the lifetime of the  $6s6p^1P$  level, no quenching would be observed. If it is much smaller, the fluorescence signal should follow a Poisson distribution of zero order,  $P_0(<n>) = \exp(-<n>)$ , when varying the average number  $<n>$  of methane molecules *per* cluster. The situation met by Lallement *et al.* fall between these extremes, indicating that quenching and radiative decay are in competition. Hence, the lifetime of the  $6s6p^1P$  level can be used as a clock to estimate the collision time between Ba and CH<sub>4</sub> in the cluster environment. Actually, the kinetic model developed by Lallement *et al.* is grounded on the sole competition between quenching and radiative lifetime. It ignores that in a finite medium, Ba and CH<sub>4</sub>, even if not associated permanently, may be close enough to shift the  $Ba(6s6p^1P \leftarrow 6s^2^1S)$  absorption out of resonance with the laser. A more refined model was proposed by Briant *et al.* and applied to situation where Ba and CH<sub>4</sub> are deposited on Ar and Ne clusters.<sup>89</sup> The model was thought as a transposition of chemical thermodynamics to finite size media. It had two parameters, which were determined by fitting the experimental data: the percentage of association between Ba and CH<sub>4</sub> and the collision time  $\tau$  between non-associated Ba and CH<sub>4</sub> partners, respectively found to be 0.05 and  $17 \pm 2$  ns in Ar <sub>$\approx 1000$</sub>  clusters. When varying the size of the cluster,  $\tau$  was found to scale as the cluster surface and was related in Ref. 89 to a diffusion coefficient, a cluster-size independent quantity. This was achieved by applying the very general theory developed by Tachiya and coworker for diffusion controlled reactions on spherical surfaces.<sup>90</sup> The value of the relative diffusion coefficient between Ba and CH<sub>4</sub> found in Ref. 89 was  $2.8 \times 10^{-6} \text{ cm}^2\text{s}^{-1}$ . It corresponds to the diffusion of CH<sub>4</sub>, essentially. As a comparison, the self-diffusion coefficient inside solid argon is orders of magnitude smaller ( $\approx 5 \times 10^{-26} \text{ cm}^2\text{s}^{-1}$  when extrapolating the data of Ref. 91 at 35 K, the cluster temperature).

Interestingly, Gaigeot *et al.* ran molecular dynamics calcula-

tions to simulated the movement and aggregation of one and several N<sub>2</sub>O molecules at the surface of Ar<sub>125</sub> and Ar<sub>147</sub> clusters.<sup>55</sup> Diffusion coefficients in the range  $4-100 \times 10^{-7} \text{ cm}^2\text{s}^{-1}$  were found. The order of magnitude is similar to that found above for the relative diffusion coefficient between Ba and CH<sub>4</sub> on argon clusters. Here, the outer shell of Ar<sub>125</sub> is not complete and the N<sub>2</sub>O molecule makes a random walks, hopping from one argon lacuna to the other at the cluster surface. A similar computational approach to diffusion coefficients has been proposed by Mukamel.<sup>92,93</sup>

Renewed interest to this field has appeared with the spectroscopy work of Dvorak *et al.* on 3, 4, 9, 10-Perylenetetra-carboxylic Dianhydride.<sup>94,95</sup> Apparently, no mobility of this large molecule was observed at the surface of an argon cluster and, when several such large molecules were present on the same cluster, they stayed isolated from each other. This contrasts dramatically with the behaviour of atoms and small molecules recalled above. These two extreme situations emphasize that mobility at the surface of heavy rare gas clusters has no general answer yet and must be examined on a case-by-case basis. Its full modeling is certainly an interesting challenge, especially when considering molecular clusters where many body effects play a role (*e.g.* water clusters that can build a network of hydrogen bond).

## 5 Photoinduced dynamics of pure and doped rare gas clusters

The present section and the following ones address a fundamental process: structural and energy relaxation within photoexcited nano-systems, driven by couplings between numerous electronic and geometrical degrees of freedom. Here, processes that follow the absorption of a photon by the constituents of a rare gas cluster (or helium nanodroplet) are considered. Four situations are examined. In subsections 5.1 and 5.3, the electronic relaxation is entirely driven by deformations of the cluster/droplet. In subsections 5.2 and 5.4, a guest molecule participates to the last steps of the energy relaxation.

### 5.1 Exciton relaxation within pure heavy rare gas clusters

The response of pure clusters of heavy rare gases to photoexcitation has been investigated since the late 1980's.<sup>96-98</sup> It was immediately recognized that electronic excitation of the cluster necessarily induces its structural reorganization.<sup>97</sup> The equilibrium structure of rare gas clusters is indeed very different, whether the cluster is in the ground-state or electronically excited. This difference is related to the equilibrium distance in rare gas dimers, much larger in the ground state than in bound electronically excited states, (*e.g.* 0.38 nm *versus* 0.25 nm for the argon dimer).<sup>99,100</sup> The former is dominated by weak van der Waals forces whereas the latter, because the excited state has a significant Rydberg character, is controlled by a much stronger chemical bond.

In short, the excited states of clusters can be thought of as bound electron-hole pairs,<sup>15</sup> described by the Wannier or by the Frenkel exciton model.<sup>101,102</sup> Given the strong dynamical

effect suggested above, the *free excitons* that are populated initially when the clusters still have the ground state structure likely evolve toward *self-trapped excitons* when the cluster atoms rearrange toward a relaxed structure.<sup>97</sup> Of course, such a dynamics is expected in rare gas solids, also. It has been documented in solid argon by Savchenko *et al.* who demonstrated that self-trapped excitons form molecular states within the solid and plays a key role in the formation of permanent electronically induced lattice defects (Frenkel pairs).<sup>103</sup> Turning back to argon clusters, localization of electronic excitation into molecular states has been predicted by the diatomics-in-molecules (DIM) calculations of Naumkin and Wales.<sup>104</sup> The lowest energy structure of electronically excited  $\text{Ar}_n$  clusters ( $3 \leq n \leq 25$ ) was determined, showing that the excitation is localized in a triatomic core, similarly to the charge in  $\text{Ar}_n^+$  ions. However, only one end of the excited core is solvated by the other atoms of cluster.<sup>104</sup> This suggests that, after a free exciton is formed somewhere in an argon cluster, it migrates toward the cluster surface and relaxes as a molecular self-trapped exciton.

A process of this type has been investigated in the real-time domain by Lietard *et al.*<sup>105</sup> A pump-probe femtosecond experiment was performed where argon clusters were excited to a Wannier exciton at 14 eV by a three photon absorption of the pump laser pulse at 265.5 nm. The probe laser pulse, operating at 796.5 nm, ionized the electronically excited clusters in a single or two photon process, after an adjustable delay with the pump laser pulse. The resulting photoelectrons were recorded using a Velocity Map Imaging Spectrometer (VMI)\* as a function of the pump-probe time delay. This achieved a Femtosecond Time-Resolved Photo-Electron Spectroscopy (TRPES) experiment.<sup>108</sup> This provided Lietard *et al.* with a series of photoelectron spectra as a function of the pump-probe time delay. They are shown in Fig 1. The important observation is the two parallel bands, which are highlighted by white dotted lines in the Figure. The intense band of lower energy probes the excited clusters in a single-photon ionization process whereas the other band probes the same state in a two-photon process. This observation was interpreted in Ref. 105 as the time dependent formation of a molecular self-trapped exciton whose centre energy decreases linearly as a function of time with a  $0.59 \pm 0.06 \text{ eV} \cdot \text{ps}^{-1}$  rate.

A crude model of the evolution was developed in Ref. 105, also. It was broadly inspired by the network of curves calculated by Duplaa and Spiegelmann to describe the excited states of the  $\text{Ar}_2$  dimer.<sup>100</sup> It is very close to that developed by Verlet *et al.* to treat of the time-resolved electron-nuclear relaxation dynamics in intraband excited Hg clusters.<sup>109</sup> Here, a cascade between neighbouring states was assumed within a manifold of equally spaced electronic states. The accessible density of states is actually very large, owing to the large number of atoms over which the electronic energy can be delocalized. The model predicted (see supplementary information in Ref. 105) a linear decay of the

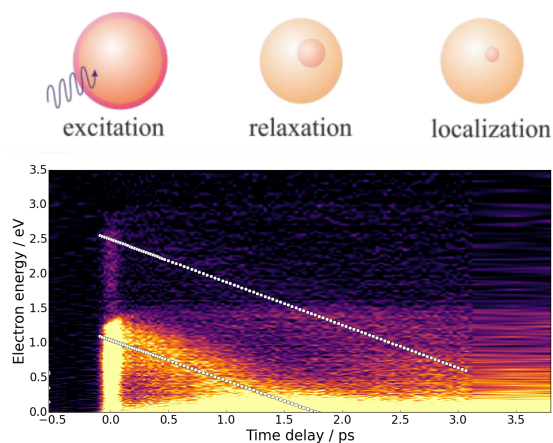


**Fig. 1** Bottom panel: photoelectron spectra (vertical axis) versus the pump (265.5 nm) - probe (796.5 nm) time delay. The colors, from dark to hell, indicate increasing signal intensities. The white dotted lines guide the eyes along the two bands whose centre energy decreases at increasing time delays. Top panel: cartoon showing three steps in the exciton dynamics. Adapted from Ref. 105 with permission from the PCCP Owner Societies.

electronic excitation in agreement with experiment, suggesting that the decay lasts  $5.1 \pm 0.7 \text{ ps}$  (only the first 3 ps of this evolution appears in the time window of the experiment, see Fig 1). This value falls in the same range as that found by Peterson *et al.* in a picosecond transient absorption spectroscopy experiment where the dynamics of exciton tunneling and trapping is studied in condensed xenon over the density range  $0.1\text{-}1.8 \text{ g} \cdot \text{ml}^{-1}$ .<sup>110</sup>

Interestingly also, relaxation time measurements were reported by Serdobintsev *et al.* in small electronically excited xenon clusters.<sup>111</sup> Among other nonradiative relaxation processes, electronic relaxation towards a self trapped exciton was observed in  $\text{Xe}_{>10}$  clusters following a two photon excitation at 263 nm (9.4 eV). In similarity with the argon experiment reported in Fig. 1, a linear decay of the electronic energy was observed as a function of time. Its rate,  $0.075 \text{ eV} \cdot \text{ps}^{-1}$ , is almost an order of magnitude smaller than that reported above in the argon experiment. This is expected actually. The decay model that has just been reported shows indeed that this decay rate scales as  $\frac{k}{\rho}$  where  $k$  is the decay rate between adjacent electronic states and  $\rho$  the density of states. When switching from argon to xenon environments, the former scales as the mass ratio between argon and xenon and the latter as its inverse. Hence, the decay rate of the electronic energy measured in the argon ( $0.59 \text{ eV} \cdot \text{ps}^{-1}$ ) and xenon ( $0.075 \text{ eV} \cdot \text{ps}^{-1}$ ) environments must scale as  $\left(\frac{M_{\text{Ar}}}{M_{\text{Xe}}}\right)^2 = 0.17$ , which is approximately the case.

Note that electronic excitation in heavy rare gas clusters that was just reviewed does not lead to bubble formation, in contrast with the situation that we shall see below in helium nanodroplets (Sec. 5.3). However, bubbles formation has been reported in solids of heavy rare gases when the electronic excitation is carried by a guest molecule, for instance, upon excitation of the  $A(3s\sigma)$  Rydberg orbital of NO in solid neon.<sup>112-114</sup>

\* The Velocity Map Imaging imaging technique was first developed by Eppink and Parker.<sup>106</sup> Its principle is reviewed in Ref. 107 where its newer developments, e.g. Covariance-Map Imaging, are described

## 5.2 Penning ionization within doped clusters of heavy rare gases

The relaxation of free excitons changes very significantly when a guest molecule is present in the cluster. The ionization energy of the latter is likely smaller than the electronic energy, which is carried by the exciton. An energy transfer is therefore possible, where the guest molecule is ionized.

A process of this type has been explored experimentally and documented theoretically by Musahid Ahmed and coworkers in  $\text{Ar}_{\sim 20}$  clusters hosting either  $(\text{H}_2\text{O})_{1-9}$  complexes or a  $\text{C}_2\text{H}_2$  molecule.<sup>115,116</sup> The experiments were performed on the Chemical Dynamics beamline at the Berkeley Advance Light Source (ALS).<sup>29</sup> The clusters were generated by continuous supersonic expansion of argon mixed with guest molecules. The beam source was coupled to the three-metre VUV monochromator of the ALS. The resulting ions were monitored as a function of the VUV wavelength using a reflectron time-of-flight (TOF) mass spectrometer. This provided Musahid Ahmed and coworkers with photoionization efficiency (PEI) curves. Although the argon clusters were fairly small, the resemblance between the appearances of the PIE curves with the excitation spectra of  $\text{Ar}_n$  clusters was striking, indicating that an exciton is formed prior ionization of the guest molecules. A parallel was made by Musahid Ahmed and coworkers with the Penning ionization process, which study dates back to the early age of reaction dynamics: an excited atom  $\text{A}^*$  and a partner  $\text{M}$  form an electronically excited collision complex  $(\text{A} \cdots \text{M})^*$ .<sup>117</sup> Recent developments concerning the stereodynamics of the Penning ionization process were reviewed by Falcinelli *et al.*<sup>118</sup>

Musahid Ahmed and coworkers noted a very interesting dynamical feature when the Penning ionization occurs within a cluster: the evaporation of the surrounding argon atoms cools down the newly formed ion, which can be stabilized under a metastable structure (*e.g.* unprotonated water cluster ions).<sup>115</sup> From a theoretical point of view, this offers a splendid benchmark for those, as Calvo *et al.*, are interested in modeling multiscale dynamical behaviours with timescales ranging from atto or femtoseconds to milliseconds and even much more.<sup>119</sup> From this point of view, it is interesting to bring together the situation just recalled above from the work of Musahid Ahmed and that reported in the previous section from the work of Lietard *et al.*<sup>105</sup> on large argon clusters. This rises the question of Penning ionization dynamics that, to our knowledge, has not been investigated yet in time resolved experiment. Since the initial exciton state is delocalized on the cluster, the Penning ionization can be thought either as a direct electronic coupling between the molecule and the delocalised free exciton, or as a sequential process where a self-trapped exciton is formed and migrates towards the molecule.

## 5.3 Photoinduced dynamics within pure helium nanodroplets

The studies reported in the present section belong to a general concern where helium nanodroplets, which appear as nearly ideal matrices for microwave and infrared spectroscopy, develop actually invasive dynamical effects when electronic excitation or ion-

ization is present. In this context, strong host-guest forces are at play and guest-helium exciplexes, ionic complexes (snowballs) or even nanoplasmas can be formed.<sup>120</sup>

An excellent overview of the intrinsic behaviour of electronically excited helium nanodroplets, about 15 years ago, is given in Ref. 121. Experimental works in both the energy and time domains are reviewed, with special focus on the latter. Information is provided on the surface and bulk dynamics of the nanodroplets that follows electronic excitation. Broadly speaking, electronic excitation in nanodroplets can be considered as fairly localized. The associated dynamics includes interband relaxation, formation of transient excited molecular complexes inside the nanodroplets and ejection of Rydberg atoms ( $\text{He}^*$ ) and molecules ( $\text{He}_n^*$ ). The work of Mudrich *et al.* reported below is a further step in this direction. It offers real-time information on the formation of bubbles around electronically excited helium atoms or molecules, a phenomenon that was reported for first time by von Haeften *et al.*<sup>122</sup>

Mudrich *et al.* have run experiments on helium nanodroplets in the same spirit as those reported in Sec. 5.1 where the dynamics of a Wannier exciton in an argon cluster was followed until it becomes a self-trapped exciton.<sup>31</sup> The helium nanodroplet experiments were performed on the low density matter end-station of the FERMI free-electron laser at the Elettra facility in Trieste. Helium nanodroplets (size ranging between  $2 \times 10^3$  and  $3 \times 10^8$  helium atoms) were excited between 21.0 and 22.2 eV within the strong absorption band, which is associated with the state manifold that correlates to  $\text{He}(1s2p^1\text{P})$ . The resulting dynamics was probed by ionization at 4.8 eV and the photoelectrons were monitored with a VMI as in the argon experiment reported in Sec. 5.1.

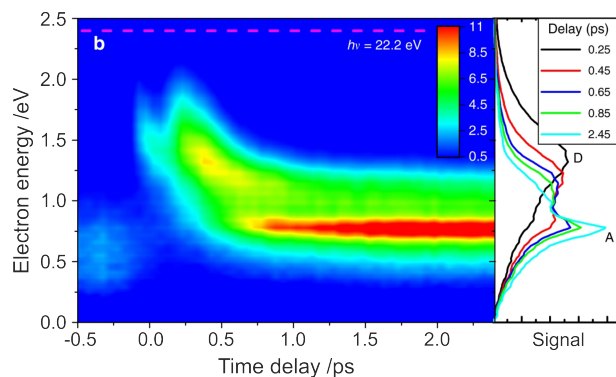


**Fig. 2** Left panel: photoelectron spectra (vertical axis) versus the pump (21.0 eV) - probe (4.8 eV) time delay. The signal intensity is shown by the color scale in the inset. Right panel: cut through the left panel image at selected time delays given in the inset. The photoelectron signal (horizontal axis) is shown as a function of the photoelectron energy (vertical axis). Adapted from Ref. 31 (Licence CC-BY 4.0)

Part of the results obtained by Mudrich *et al.* are reproduced in Fig. 2. The electron spectra are dominated at short time delays ( $t \lesssim 0.5$  ps) by the broad feature labeled "D" in the right panel of the figure. Its centre energy decreases as a function of time. At longer time delays the sharp peak labeled "A" appears, partly at the expense of feature "D". Bringing together these observations with He-TDDFT calculations performed in the same work, *ab-*

*initio* molecular dynamics calculations reported in Ref. 123 and earlier photoluminescence studies,<sup>124</sup> Mudrich *et al.* proposed a three step scenario for whole process: (i) the initial electronic excitation, likely delocalized over several He atoms, is relaxed toward the lowest excited band of the droplet (that built from the He(1s2s<sup>1</sup>S states) within less than 250 fs. (ii) Further relaxation proceeds with formation of a bubble in  $\approx 0.5$  ps about an excited He\* atom. The bubble formation is due to the Pauli repulsion between the excited electron and the electrons of the filled orbitals of the surrounding ground state helium atoms. (iii) Then, the bubble migrates to the nanodroplet surface and bursts to release a free metastable He\* atom. This step is fairly slow, 2.5 ps. Its completion strongly depends on the location of the initial electronic excitation, whether it is close to the surface or deeper inside the droplet.<sup>31</sup>

#### 5.4 Penning ionization within helium nanodroplets

The Penning-like ionization process that has just been reviewed in argon clusters has been observed in Helium nanodroplets also.<sup>125–127</sup> The guest species were heavy rare gases (Ref. 125) and organic molecules (Refs. 126,127). For instance, Mandal *et al.* considered the ionization of acetylene oligomers following photoexcitation of the n=2 and n=4 bands of He nanodroplets in electron-ion coincidence experiments.<sup>127</sup> It appears from Ref. 127 that the n=2 band acts as the energy reservoir in helium nanodroplets, in the same way as the He(1s2s<sup>3,1</sup>S) metastable states in conventional Penning ionization.

## 6 Photoinduced dynamics of a single atom hosted in clusters: benchmarks of coupled electronic and structural dynamics

This and the following section focus on an opposite situation as that encountered in Secs. 5.2 and 5.4. Here, the guest particle (and not the host) carries the initial photoexcitation and relaxes excess energy towards the host. Hence, no delocalization of the electronic excitation over several sites need to be considered as initial step of the dynamics. Guest atoms are considered in the present section.

An alkali atom or an alkaline-earth atom interacting with a rare gas cluster/droplet is among the simplest guest-host systems where to investigate the energy relaxation processes that follow electronic excitation of the guest. Obtaining detailed experimental information in this field, including information in the real-time domain is not especially difficult given the nowadays developments in the beam and laser spectroscopy techniques. This will be exemplified in the examples reported below. The challenge is on the theoretical side. Because of its apparent simplicity, this issue appears indeed as a benchmark where to develop theoretical approaches that face the full complexity of coupled electronic and structural relaxation.

#### 6.1 Valence excitation of a hosted alkali atom

**Alkali atoms hosted in quantum media (helium nanodroplets and *para*-H<sub>2</sub> clusters** - Laser induced fluorescence (LIF) and

Laser induced beam depletion (LIBD) spectroscopy of alkali atoms hosted in quantum media (helium nanodroplets and *para*-H<sub>2</sub> clusters) has been investigated very early in the group of G. Scoles.<sup>128</sup> The LIF and LIBD spectra are very different from each other in the *para*-H<sub>2</sub> experiment, suggesting that non radiative processes dominate the guest-host dynamics. This is not the case in helium nanodroplets. Further studies of the same group showed that the guest-host dynamics in helium nanodroplets results in the formation and ejection of Alkali-Helium exciplexes (e.g. Na\*-He and K\*-He), the alkali atom being initially solvated near the nanodroplet surface.<sup>129–131</sup> Some ambiguity exists regarding the time scale of the formation/ejection of the K\*-He exciplex.<sup>130,132,133</sup> Nevertheless, a theoretical description, consistent with the observation of Reho *et al.* in Refs. 129,130 has been developed by Martinez *et al.* using the helium density functional method (He-TDDFT) to describe the nano-droplet and either a classical or quantum description of the K-atom dynamics within the droplet.<sup>134</sup>

States are labeled according to a pseudo-diatom picture of the K ··· droplet interaction where the nanodroplet is represented as a pseudo-atom. This picture is justified by the shape of the LIF and LIBD spectra reported by Scoles and coworkers in Ref. 128: a clear  $\Sigma - \Pi$  splitting corresponding to the alignment of the 4p orbital, either perpendicular or parallel to the droplet surface. The calculation of Martinez *et al.* shows that excitation to the  $4p^2\Sigma_{\frac{1}{2}}$  pseudo-diatom state leads impulsively to the ejection of K in the  $4p^2P_{\frac{3}{2}}$  atomic state. Excitation to  $4p^2\Pi_{\frac{3}{2}}$  leads to the formation of the K(4p<sup>2</sup>P)-He exciplex through a no-barrier pathway.<sup>134</sup> Excitation to the  $4p^2\Pi_{\frac{1}{2}}$  state induces a complicated dynamics because an energy barrier is present along the  $4p^2\Pi_{\frac{1}{2}}$  curve. This prevents direct formation of the K(4p<sup>2</sup>P)-He exciplex and makes the K atom bouncing within a shallow well of the potential curve. With the two later excitations, the K(4p<sup>2</sup>P) atom interacts with helium for a long time. This stimulates spin-orbit (SO) relaxation (as in collision induced fine-structure transitions)<sup>135</sup> and enables stabilization of ring exciplexes. The corresponding helium density is shown in Fig. 3 for the  $4p^2\Pi_{\frac{1}{2}}$  excitation.

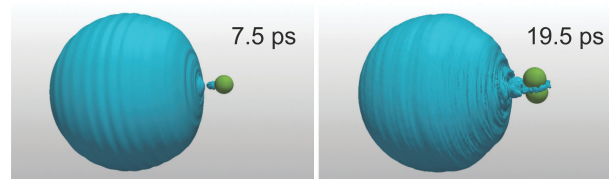


**Fig. 3** Snapshots taken from the calculations in Ref. 134. They show the helium density in (He)<sub>1000</sub> nanodroplets carrying a single K atom after excitation of the K atom to the  $4p^2\Pi_{\frac{1}{2}}$  state. The left (resp. right) picture is taken before (resp. after) the spin-orbit relaxation mentioned in the text has proceeded. Adapted from Ref. 134 with permission from the PCCP Owner Societies.

The ejection dynamics of a Rb atom out off the surface of helium nanodroplets has been investigated also in a combined experimental and theoretical approach as above.<sup>133,136,137</sup> The valence excitation of the Rb atom promotes an evaporation-like process rather than an impulsive desorption. Again, spin relaxation

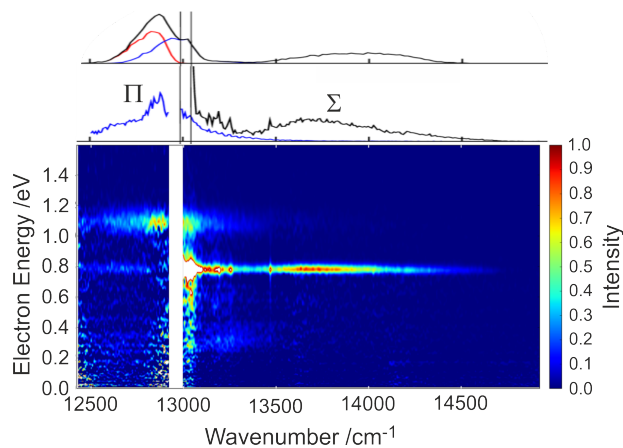


**Fig. 4** Correlation plot (bottom panel) between the photoelectron energy (vertical scale) and the pump-photon energy (horizontal scale). The intensity of the photoelectron signal is given by the colour scale (in arbitrary units). The black spectrum in the middle panel focuses on the photoelectrons associated with free K atoms, ejected from the cluster. The blue spectrum in the same panel focuses on K atoms that remain bound to the cluster. The black curve in the top panel shows the simulated total absorption spectrum and the red (resp. blue) curve absorption towards the  $\Pi_{1/2}$  (resp.  $\Pi_{3/2}$  state). Adapted with permission from Ref. 56. Copyright © 2015 American Chemical Society.

stimulates desorption of a long lived Rb-He exciplex.

**Non-quantum hosts (argon clusters)** - The latter remark interrogates on the role played by the SO coupling in the dissociative dynamics of excited alkali atoms from helium nanodroplets and more generally from rare gas clusters. This question has been examined theoretically by Gervais *et al.* for small  $M(\text{Ar})_n$  clusters ( $n=1-6$ ,  $M=\text{Li-Rb}$ ).<sup>138</sup> Small SO coupling is associated with an essentially diabatic dynamics, which becomes more and more adiabatic as the SO coupling increases. The centre point of the work was the theoretical method which allowed treating in one shot, energy, forces and non-adiabatic couplings in systems that carry a fairly large number of electronic and structural degrees of freedom. An effective one-valence-electron model was used, all other electrons being incorporated in pseudopotentials about the polarizable  $M^+$  and Ar cores.

To step further into the photoinduced dynamics of alkali atoms hosted in non-quantum clusters, Douady *et al.* performed a combined experimental and simulation study where a single K atom bound to the surface of an  $\text{Ar}_n$  cluster was electronically excited to states correlating with the first doublet state ( $4p^2P$ ) of free potassium.<sup>56</sup> Resonance Enhanced MultiPhoton Ionization-PhotoElectron Spectroscopy (REMPE-PES) experiment was performed as described in Ref. 139. The photoelectron spectra provided by the REMPE detection were monitored as a function of the energy of the pump-photons that excite the K atoms. The experimental results are summarized in the two bottom panels of Fig. 4. As above in the helium droplet experiments, the pseudo-diatomic picture is used to label the energy states.

The experimental spectra, which appear in the middle panel of Fig. 4 exhibit two broad bands. The black band labeled  $\Sigma$ , in the blue side of the spectrum, is associated with perpendicular

alignment of the  $4p$  orbital with respect to the cluster surface, whereas the partly structured  $\Pi$  band corresponds to the parallel alignment of the same orbital. The  $\Sigma - \Pi$  splitting is significantly larger than observed in Ref. 128 when K is attached to a helium nanodroplet. Surprisingly, a large amount of the K atoms that are picked-up by the cluster are subsequently lost and reach the interaction zone with the pump laser as free K atoms. The corresponding signal is the saturated white area broadly centred at the ( $13,023 \text{ cm}^{-1}$ ,  $0.77 \text{ eV}$ ) coordinates in the bottom panel of the figure. The other clear message from the experiment is that the excitation within the broad  $\Sigma$  band leads to the formation of free K atoms (revealed by the intense narrow feature at  $0.77 \text{ eV}$  in the photoelectron spectra that extends over the whole  $\Sigma$  band when scanning the pump-photon energy). In contrast, excitation in the  $\Pi$  band leads to the formation of a bound state.<sup>56</sup>

These observations and the experimental photoelectron spectra were quantitatively reproduced in Ref. 56 by a nonadiabatic molecular dynamics simulation of a  $\text{K}(\text{Ar})_{731}$  cluster (compare the top and middle panels of Fig. 4). Among other information, the calculation showed that relaxation of the  $\Pi$  excitation drives the system toward a basin where the coordination of the K atom is 2.2 Ar atoms on the average, in a poorly structured surface.<sup>56</sup>

## 6.2 Valence state excited alkaline-earth atoms

With two valence electrons, alkaline earth atoms offer a more complex electronic landscape and therefore a richer photoinduced dynamics than alkali atom, even for excitation within the state manifold correlating to the first resonance state of the free atom. For example, singlet-to-triplet energy transfers can be at play.

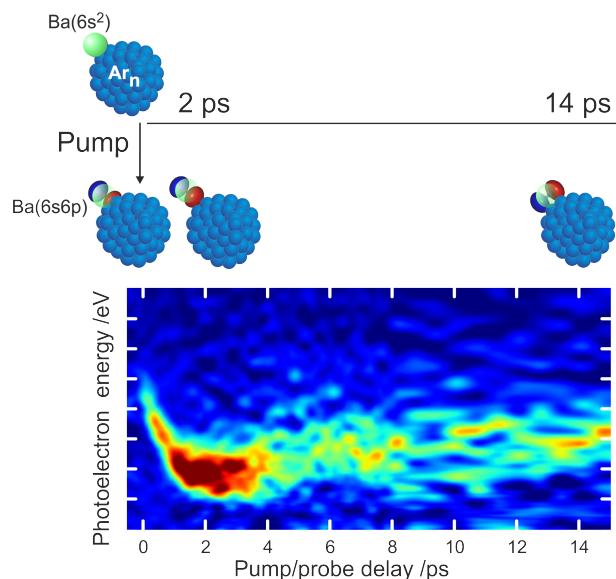


**Fig. 5** Photoelectron spectra of electronically excited  $\text{Ba}(\text{Ar})_{\approx 500}$  clusters as a function of the pump-probe delay in the TRPES experiment. A  $\Sigma$ -like excitation toward the  $^1P$ -manifold was performed by the pump-laser at time  $t=0$ . The signal intensity is given in false colors (zero intensity in dark blue and increasing intensities in light blue, green, yellow, red and brown, respectively). Same color map as in Fig. 4. Adapted from Ref. 57 with permission from the PCCP Owner Societies.

Awali *et al.* investigated the dynamics of an electronically excited barium atom deposited at the surface of an  $\text{Ar}_{\approx 500}$  cluster. Information was collected from frequency-resolved nanosecond experiments (REMPI-PES experiments as recalled above when reviewing Ref. 56) and from femtosecond time-resolved experiments (TRPES experiments as seen above when reviewing Ref. 105).<sup>57</sup> Barium was electronically excited within the  $^1\text{P}$ -manifold which correlates to the resonance state  $6s6p\ ^1\text{P}_1$  of free barium. The resulting dynamics either left the excitation within the initial  $^1\text{P}$ -manifold (main channel) or brought it to the  $^3\text{P}$ -manifold correlating to  $\text{Ba}(6s6p^3\text{P})$ . In both cases, there was a competition between ejection and solvation of the barium atoms. Fig. 5 reports a striking time-resolved information from Ref.<sup>57</sup>. It follows a  $\Sigma$ -like excitation toward the  $^1\text{P}$ -manifold in a situation where barium stays solvated within the cluster and does not switch to the  $^3\text{P}$ -manifold. The cartoon shows the interpretation, where the initial  $\Sigma$ -like alignment of the  $\text{Ba}(6p)$  orbital is relaxing to the  $\Pi$ -like alignment while barium makes a large amplitude oscillation with respect to the cluster surface, the oscillation being damped very rapidly. The oscillation period is *ca* 4 ps. The bouncing movement of barium is associated with a variation of the photoelectron energy because the electronically excited surface that is probed is not parallel to the ionic surface onto which it is projected. This interpretation stems from the molecular dynamics simulation with electronic mode hopping developed by Heitz *et al.* in a similar system where the barium atom is replaced by calcium and the icosahedral-like cluster  $\text{Ar}_{54}$  is considered.<sup>140</sup> The results by Heitz *et al.* are recalled in Fig. 6. The bottom panel of this figure strikingly similar to that of Fig. 5

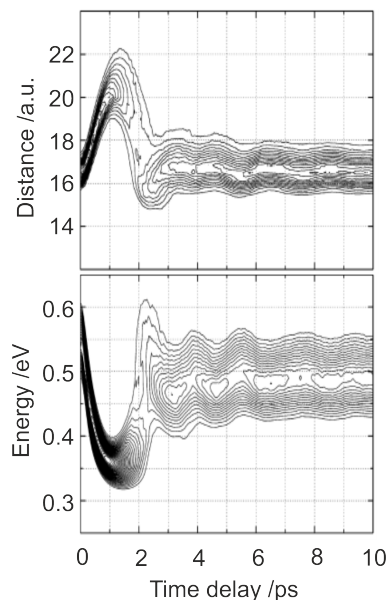


**Fig. 6** Numerical simulation by Heitz *et al.* showing the dynamics of a  $\text{CaAr}_{54}$  cluster following a  $\Sigma$ -like excitation of the Ca atom. Distance from Ca to the centre of mass of the argon cluster (Upper panel) and photoelectron spectrum (Lower panel) as a function of the pump (2.96 eV) - probe (3.50 eV) time delay (in ps). Adapted with permission from Ref. 140. Copyright © 2010 American Chemical Society.

### 6.3 Rydberg excitation of the guest atom

**Single Ba atom bound to the surface of an argon cluster** - A complex situation where many electronic and structural relaxation pathways are coupled was addressed experimentally in Ref. 58 and theoretically in Refs. 58,141. Experimentally,  $\text{BaAr}_{\approx 750}$  clusters were excited in the vicinity of the  $6s9p\ ^1\text{P}$  state of free

barium and probed by ionization in a femtosecond pump/probe scheme. The velocity imaging (VMI) technique was used to monitor the energy distribution of photoelectrons and photoions as a function of the time delay between the pump and probe pulses. On the theoretical side, mixed quantum-classical dynamics was used to account for the nonadiabatic transitions among more than 160 electronic states. A diatomics-in-molecules (DIM) approach allowed for an efficient calculation of the Hamiltonian matrix and its gradients, whereas an Ehrenfest-based method enabled propagation in a diabatic basis. To bypass troubles with an inappropriate mean-field potential when the forces on several electronic states are very different, the electronic wave packet was collapsed onto a single adiabatic surface at regular time intervals, hence applying the "mean field with quenching" (MFQ) method described by Janecek *et al.*<sup>142</sup>

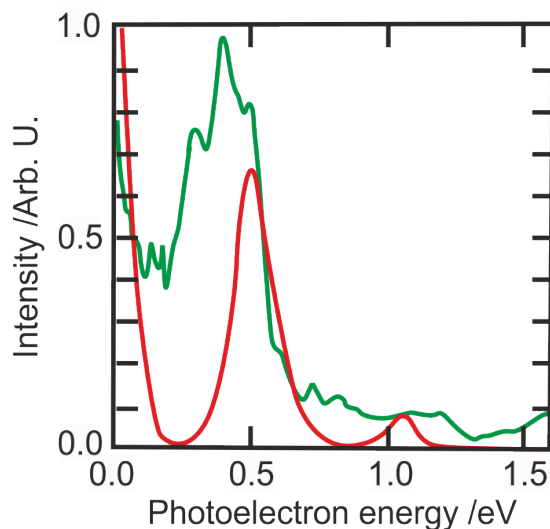


**Fig. 7** Comparison between simulated (red curve; data taken from Ref. 141) and experimental (green curve; data taken from Ref. 58) photoelectron spectra of  $\text{BaAr}_n$  clusters at long pump-probe time delay after excitation of barium in the vicinity of the  $6s9p\ ^1\text{P}$  state of free barium.

Dynamics on singlet potential energy surfaces was considered in the calculation of Ref. 141. This significant simplification avoided including spin-orbit coupling when simulating the ionization probe signal. Hence, only qualitative agreement with experiment is to be expected as observed in Fig. 7. Importantly, the simulation reflects the multimode nature of the experimental spectrum, a fingerprint that at least two relaxation pathways are at play. They differ by the dominant electronic configuration of the final state after energy relaxation,  $\text{Ba}(6s6p)\text{Ar}_n$  or  $\text{Ba}(6s5d)\text{Ar}_n$ . In agreement with experiment, the simulation shows that the Rydberg excitation of the  $\text{BaAr}_n$  clusters by the pump laser leads first to embedding of barium inside the cluster, as a  $\text{Ba}^+\text{Ar}_n$  core surrounded by a diffuse electron. Subsequently, the coupling of electronic and vibrational motion induces a cascade of nonadiabatic transitions down to the  $\text{Ba}(6s6p)\text{Ar}_n$  or  $\text{Ba}(6s5d)\text{Ar}_n$  states, along with back migration of Ba towards the surface of the cluster for the  $\text{Ba}(6s6p)\text{Ar}_n$  channel essentially. Surprisingly, no ejection of atomic barium appeared in the simulation although ejection was observed experimentally.

The ejection of barium atoms, which was observed experimentally, was interpreted as a delayed, very indirect slow process. Ejection did not proceed during the first 5 ps of the dynamics. This was interpreted as a peculiarity of pump-probe experiments where the probe operates by ionization. At short time delay indeed, barium atoms that are to be ejected as neutral atom have not enough kinetic energy and are not far enough from the argon environment to compensate the attractive interaction that appears with the argon cluster when ionized by the probe laser. Hence, upon ionization by the probe laser the newly formed  $\text{Ba}^+$  ion stays solvated within the cluster.<sup>58</sup> We shall see in the next section that this behaviour has been identified in helium droplet also. It has been called "fall-back dynamics" to point out that the ion, which should have left the cluster, is actually "call back" by the electrostatic interaction and "falls back" onto the cluster.

**The fall-back dynamics of photoions in femtosecond pump-probe experiments** - The fall-back dynamics of the photoion produced by the probe laser that has just been encountered and defined in argon clusters has been observed in quantum clusters also. It was very nicely documented by Mudrich and coworkers who investigated the real-time dynamics of a single excited rubidium atom attached to helium nanodroplets.<sup>133</sup> The work combined a standard femtosecond pump-probe experiment with simulations based on He-TDDFT theory. A Rb atom bound to a He nanodroplet was excited to states correlating to the  $5p^1P$  and  $6p^1P$  states of free Rb. The dynamics was probed by ionization of  $\text{Rb}^*$  and the resulting ions were monitored as a function of the pump-probe time delay. The simulations performed in this work documented the movement of  $\text{Rb}^*$  after the pump excitation and the subsequent movement of the  $\text{Rb}^+$  ion after  $\text{Rb}^*$  was ionized by the probe laser. The fall-back dynamics of the  $\text{Rb}^+$  ion is particularly well illustrated by the first animation in the series of four that are available in the Supporting Information of Ref. 133. The animation shows a rubidium atom, which starts desorbing after excitation to the  $5p\Pi_{1/2}$  state at time zero. It is ionized 20 ps later before it fully exits the droplet. At that point, the fall-back dynamics begins.

**Rydberg states in heavy rare gas clusters and helium nanodroplets** - The dynamics immediately following the Rydberg excitation of  $\text{BaAr}_n$  clusters was interpreted in Ref. 58 and documented numerically in Ref. 141 as the formation of a  $\text{Ba}^+\text{Ar}_n$  core surrounded by a diffuse electron, the latter being especially diffuse when the core  $\text{Ba}^+$  has the 6s electronic configuration.

This picture, which concerns Rydberg states of small principal quantum number, has similarities with observations reported by Marcel Drabbels and coworkers for much higher Rydberg states in the context of quantum helium nanodroplets.<sup>143,144</sup> Excitation spectra of sodium-doped helium nanodroplets were recorded up to the ionization limit. A series of Rydberg-like bands were observed and interpreted as originating from a positively charged  $\text{Na}^+$  Helium-droplet core with an orbiting electron. Those with principal quantum number  $n < 20$  are found unstable at the nanosecond time scale with respect to electron-ion recombination. Those with  $n > 100$  have a lifetime larger than  $1.1\mu\text{s}$ . An issue in Ref. 143 and also in works of Wolfgang Ernst and

coworkers where Na was replaced by Cs and Rb,<sup>145,146</sup> was to model the interaction of the Rydberg electron with the ion core. Since a ground state alkali atom is located at the surface of the helium nanodroplets, a pseudo-diatomic model where a pseudo-atom takes the place of the nanodroplet is a good starting point to describe the alkali-droplet interaction. A model of this type has been developed by Calvo *et al.* to account quantitatively for the absorption spectra of calcium-doped argon clusters.<sup>85</sup> In their work on nS, nP and nD states of Cs atoms bound to a helium nanodroplet, Wolfgang Ernst and coworkers found that the pseudo-diatomic model offered a good description of the excited states, up to  $n=10$ . However, when  $n \gtrsim 10$ , the  $\text{Cs}^+$  core is strongly attracted towards the interior of the nanodroplet.<sup>145</sup>

**Growing a bubble inside a helium nanodroplet** The guest atom considered so far, alkali and alkaline earth atoms were bound to the surface of heavy rare gas clusters and helium nanodroplets. When binding an indium (In) atom to a helium nanodroplet, Ernst and coworkers investigated a situation where the guest atom is embedded inside the nanodroplet.<sup>147</sup> A femtosecond time resolved photoelectron spectroscopy (TRPES) experiment and time-dependent density functional (He-TDDFT) theory simulations were performed for documenting the photoinduced dynamics of the In-helium droplet assembly. The following picture was unravelled. Upon electronic excitation the electron cloud of In expands. The interaction between the In excited electron and the surrounding ground state He atoms is indeed repulsive at intermediate distances because of the Pauli principle. The expanding In electron cloud pushes helium atoms away and a void bubble is forming about the In atom. A time scale of 600 fs was found. It is associated with a collective oscillation of the helium shell that is damped after a single period of 30 ps.<sup>147</sup>

## 7 Photoinduced dynamics of a single guest molecule

### 7.1 A related matter: isolation at low temperature in rare gas matrices

Let us divert a little to a related matter: isolation at low temperature in rare gas matrices.<sup>148</sup> It is known for a long time that atoms and molecules can occupy a variety of sites where one or several atoms of rare gas lattices are substituted by guest species.<sup>149,150</sup> The environment differences provided by the various trapping sites not only affects the spectroscopy of the guest species (frequency shifts) but also affects subsequent dynamics when the guest species are photoexcited.<sup>151-154</sup> An observation is especially relevant for the scope of the present perspective article: the nature of the trapping sites may be different whether the guest species (alkali atoms in argon matrices) is in the ground electronic state or electronically excited.<sup>155,156</sup> Numerical simulations provided in Refs. 155,156 show that after electronic excitation, the metal atom migrates from less to more favourable solvation sites. The alternative large deformation of the matrix around the metal atom would be too slow to be observed.

More recent experimental works based either on photon echo techniques or detection of amplified spontaneous emission show that the different solvation sites of large polyatomic molecules (ei-

ther 2D planar tetrapyrrolic molecules or 3D ball-shape molecules as  $W(\text{CO})_6$ ) are not coupled in the same way to the phonons of the rare gas lattice.<sup>157–159</sup> This paves the way to site selective dynamics studies.

## 7.2 Triethylenediamine (DABCO) molecules bound to argon clusters: quantum beats, hopping dynamics between solvation sites and orbital manipulation

This section comes back to solvation in rare gas clusters. It summarizes a ten years saga in our research group which was initiated by a collaboration with David Parker who was aware of the interesting peculiarities (recalled below) of the DABCO molecule (1,4-diazabicyclo-[2,2,2]octane or triethylenediamine, )<sup>160–162</sup> The multiscale, time-resolved, excited state dynamics of the DABCO molecule was investigated when the molecule is either free or solvated at the surface of argon clusters.<sup>61,139,163–165</sup> Although the photoexcitation of the molecule was performed in the UV range, the deposited energy was not large enough to induce bond rearrangements. Hence, situations are addressed here where the photoinduced force field intensity within the molecular guest is comparable to the interaction intensity with the host. An opposite situation will be examined in the next section.

**The DABCO molecule** - The peculiar properties of the DABCO molecule are reviewed in Ref. 163. Briefly, it is a fairly spherical ( $D_{3h}$  symmetry) molecule because of the triple bridge between the N-atoms.<sup>166</sup> Its ground state  $S_0$  has a valence character and the first excited state  $S_1$  has a 3s Rydberg character at 90%.<sup>163,164,166</sup> Because of the  $D_{3h}$  symmetry, the single photon excitation  $S_1 \leftarrow S_0$  between states of  $A_1'$  symmetry is forbidden. It is made possible through a Herzberg-Teller vibronic coupling with a  $E'$  bright state (a  $\pi$  state representation in the  $D_{3h}$  point group).<sup>167</sup> The molecule has a unitary quantum yield for fluorescence from the  $S_1$  state.<sup>168</sup> Accordingly: (i) the one-photon excitation by a polarized laser leads to a slightly polarized orbital, a fingerprint of the polarization of the vibronically coupled states; (ii) a large expansion of the DABCO electronic cloud is expected upon electronic excitation; (iii) No conical intersection establish an easy connection between the  $S_1$  and  $S_0$  states.

**Quantum beats in free DABCO** - A standard time-resolved photoelectron spectroscopy (fs-TRPES) was performed in a setup that combines a molecular beam, a Velocity Map Imager (VMI) and femtosecond pump (266.3 nm) and probe ( $2 \times 792$  nm) lasers.<sup>163</sup> The latter are linearly polarized, their directions of polarization being either parallel or perpendicular to each other. Since the VMI allows recording both the energy and the angular distribution of the photoelectrons, the full experimental information consists in a series of photoelectrons spectra documenting electron distributed as the Legendre polynomials  $P_0(\cos \theta)$ ,  $P_2(\cos \theta)$ , sometimes  $P_4(\cos \theta)$  as a function of the pump-probe time delay.

The main experimental result is reproduced in Fig. 8 for the electrons distributed as  $P_0(\cos \theta)$  (total photoelectron signal). The top panel of the figure shows that the observed photoelectron spectrum is adequately fitted by four bands labeled 2.0, 2.1, 3.0 and 3.1 in the figure. The intensity of two of them (3.0 and

3.1) is plotted in the bottom panel of the figure as a function of the pump-probe time delay. State-of-the-art *ab initio* calculations are also reported in Ref. 163. They document the  $S_0$  and  $S_1$  states of the neutral molecule and the  $D_0$  ionic state in order to help in the assignment of the observed photoelectron signals.

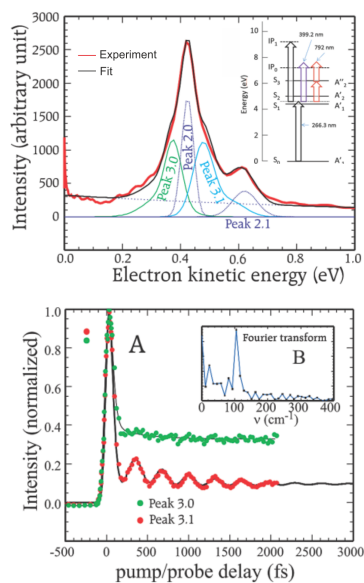


**Fig. 8** Top panel: Photoelectron spectrum of the DABCO near the zero time delay between the pump (266.3 nm) and the probe ( $2 \times 792$  nm) laser pulses. The inset shows the energetics. Bottom panel: Time evolution for two photoelectron bands provided by the fit in the top panel (bands 3.0 and 3.1). The inset shows a fast Fourier transform of the signal. Adapted with permission from Ref. 163. Copyright © 2009 American Chemical Society.

A pronounced oscillation of  $323 \pm 10$  fs is observed on band 3.1 in the bottom panel of Fig. 8. Several hypothesis were discussed by Poisson *et al.* to account for this oscillation. That which best fit with the observations and calculations of Ref. 163 and with the known vibrational spectroscopy of the DABCO molecule<sup>162</sup> is an unusual quantum interference between two vibrational modes separated by  $103 \text{ cm}^{-1}$  (likely the  $\nu_4$  and  $\nu_5$  modes of DABCO). The usual situation with vibrational quantum beats is a coherent excitation of several levels in the same vibrational mode. Here a single level in two different modes would be coherently excited. Of course, the corresponding wavepacket motion cannot be represented as a movement along a single coordinate. The fact that it is detected as an oscillation implies that at least one of the atoms of the molecule is involved in both vibrational modes (hence coupling them together) and that the detection is sensitive to the motion of this atom (achieved by the intermediate resonance in the 2-photon probe that appears in the inset of the top panel in Fig. 8).

**Hopping between solvation sites and subsequent energy relaxation: a multiscale dynamics** - Although clusters are less rigid than the rare gas matrices evoked in Sec. 7.1 and although solvation in clusters is very often surface solvation, site effects may also be encountered. The excited state dynamics of the DABCO molecule solvated at the surface of an argon cluster offers such an example.<sup>61,139,164,165</sup>

Again a joint experimental and theoretical approach was followed. On the experimental side, a single DABCO molecule was deposited by pickup on  $\text{Ar}_{\approx 5-800}$  clusters. Two different experiments were performed: Resonance Enhanced Multiphoton Ionization-Photoelectron Spectroscopy (REMPI-PES) using a nanosecond laser and femtosecond Time Resolved Photo-

electron Spectroscopy (fs-TRPES). The fs-TRPES experiment was conducted as described in the paragraph above on “Quantum beats”.  $P_0$  and  $P_2$  angular distributed photoelectron spectra were recorded as a function of the pump-probe time delay for the two relative alignments of the laser polarizations, parallel and perpendicular. On the theoretical side, a series of methods and basis sets were used (e.g. (R)MP2/aug-cc-pVXZ ( $X = D, T$ ), CASSCF/MRCl/aug-cc-pVDZ), including newly implemented explicitly correlated methods (e.g. CCSD(T)-F12a/aug-cc-pVDZ; see the review by Hochlaf)<sup>28</sup> to explore the ground and low excited ( $S_{1-4}$ ) surfaces of the DABCO<sup>0,+1</sup>-Ar<sub>*n*</sub> ( $n=1-4$ ) clusters.

The nanosecond REMPI-PES experiment revealed that the ground state DABCO molecule is in equilibrium between two solvation sites at the cluster temperature. The two sites likely correspond to a different degree of solvation by the argon atoms. Their nature is discussed in Ref. 61, taking into account the calculations of Mathivon *et al.*<sup>164</sup>. In the most solvating site, DABCO may have the N...N axis pointing towards the cluster centre. This maximizes the number of equatorial Ar-atoms which are found to stabilize the DABCO-Ar<sub>3</sub> in Ref. 164. In the least solvating site, the N...N axis could be parallel to the cluster surface with no argon atom along the N...N axis and only one or two argon atoms forming the first solvation shell.

In a 265.1 nm/399 nm pump/probe experiment as those reported in Refs. 139 and 169 the most solvating site leads to a band centred at 0.9 eV in the photoelectron spectrum recorded at a  $\tau=4$  ps pump-probe time delay, whereas the least solvating site is associated with a double band centred at 0.73 eV. All the observations in Ref. 139 indicate that excitation of DABCO to the  $S_1$  state induces hopping from the most to the least solvating site, with a timescale of 270 fs.

Observations beyond 4 ps, up to several hundred picoseconds, require attention because decoherence of the rotational alignment due to the rotation in space of the DABCO-cluster assembly falls in the range of several 100 ps. The excited orbital is indeed not purely spherical (it has only a 90% 3s Rydberg character) and is aligned by the linearly polarized pump laser. Variation of the resulting alignment as a function of the pump-probe time delay therefore combines intra-DABCO relaxation and rotational decoherence. The two phenomena were disentangled in Ref. 61.

We mentioned already that two series of experiments were performed in Ref. 61, whether the pump and probe laser polarizations are parallel or perpendicular. The photoelectron angular distribution was decomposed on the  $P_0, P_2$  basis of Legendre polynomials. A way of disentangling intra-DABCO relaxation and rotational decoherence is to consider  $P_0$  distributed electron while simulating an isotropic excitation of DABCO. This is achieved using the average quantity  $\bar{S} = \frac{S^{\parallel}(\tau) + 2S^{\perp}(\tau)}{3}$  where  $S^{\parallel}$  (resp.  $S^{\perp}$ ) is the energy spectrum of the  $P_0$  distributed photoelectrons in the experiment where the polarizations of the lasers are parallel (resp. perpendicular). A specific treatment based on information theory was performed in Ref. 61 to extract the intensity, centre energy and width of  $S^{\parallel}$  and  $S^{\perp}$  and therefore of  $\bar{S}$ , specifically for each solvating sites. Fig. 9 shows the centre energy of  $\bar{S}$  as a function of the pump-probe time delay. A very slow decay of

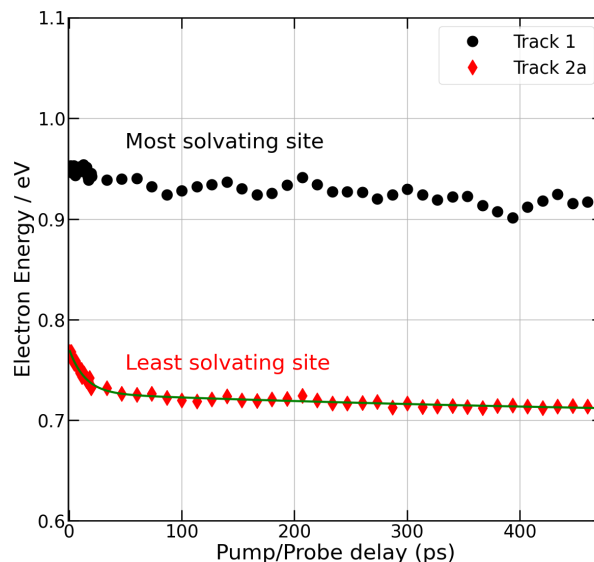


**Fig. 9** Centre energy of the bands assigned to the most and least solvating sites in an experiment simulating an isotropic excitation of DABCO-Ar<sub>*n*</sub> clusters and focusing on  $P_0$  distributed photoelectrons<sup>61</sup>. Note a small 4% discrepancy between energies reported in Table 1 and Figure 4 of Ref. 61 due to an inappropriate use of the energy calibration, it remains within experimental uncertainties.

the centre energy is observed for the most solvating site whereas the other site has a biexponential behaviour with times constants 14 ps and >150 ps. The slow process is interpreted in Ref. 61 as the relaxation time of the DABCO internal excitation to the argon bath whereas the process with the 14 ps timescale would be associated with local relaxation of the argon bath. The latter process is turned when the DABCO electron cloud is suddenly enlarged by the pump laser excitation and initiates the site hopping dynamics.

A close look to Fig. 9 may suggest that small amplitude oscillations of  $\approx 100$  fs period are superimposed on the slow decay of electron energies that has just been discussed. Similar, dimly visible oscillations are also present on the polarization anisotropy parameter, which has been built on the same data corpus in Figure 10 of Ref. 61. We consider that these oscillations, which are very close to the experimental noise, need to be confirmed prior extensive discussion.

**Double observation of polarization anisotropy and photoelectron angular anisotropy: an approach to orbital tomography?** - Anisotropies of two origins are carried by the full experimental data set of Ref. 61. **(I)** Polarization anisotropy is due to the selection of properly aligned DABCO-argon clusters by the pump laser so the oscillator strength of the transition is maximized. If the excited orbital is not spherical, it is aligned and rotates as the DABCO-argon clusters rotate. **(II)** Angular anisotropy of the photoelectrons is created by the probe process from the population and alignment of the excited state that is probed. It is described by the  $\beta_2$  parameter when the angular distribution of the photoelectrons is expanded as  $S^{\parallel \text{ or } \perp} (1 + \beta_2^{\parallel \text{ or } \perp} P_2(\cos \theta) + \dots)$ , with the same definition as above for  $S^{\parallel}$  and  $S^{\perp}$ . Note that because the Legendre polynomials form an orthogonal basis set,

$S^{\parallel}$  and  $S^{\perp}$  also represent the total photoelectron signal.

Two anisotropy parameters can be defined:  $r = \frac{S^{\parallel} - S^{\perp}}{S^{\parallel} + 2S^{\perp}}$  and  $r_{\beta} = \frac{\beta^{\parallel} - \beta^{\perp}}{\beta^{\parallel} + 2\beta^{\perp}}$ . The former  $r$  is called the polarization anisotropy parameters. In the present context of the DABCO-argon cluster dynamics at long time (*i.e.* after the site hopping dynamics is completed) the variation of  $r$  as a function of the pump-probe time delay reflects rotational coherences as described quantitatively in Ref. 61 using the formalism of Baskin and Zewail.<sup>170</sup> The other parameter  $r_{\beta}$  can be called the double anisotropy parameter. A non-zero value of  $r_{\beta}$  tells that the probed orbital is non-spherical. Since the DABCO-argon cluster rotate in space and drive the excited orbital, the latter rotates with respect to the polarization of the probe laser and is therefore probed from different directions as a function of the pump-probe time delay varies. This offers a tomographic information on the excited orbital. However, Ref. 61 discussed that the sole experiment cannot provide this information specifically because it is obscured by the slow dynamics of the DABCO<sup>+</sup> core underneath the excited orbital, within the solvation site.

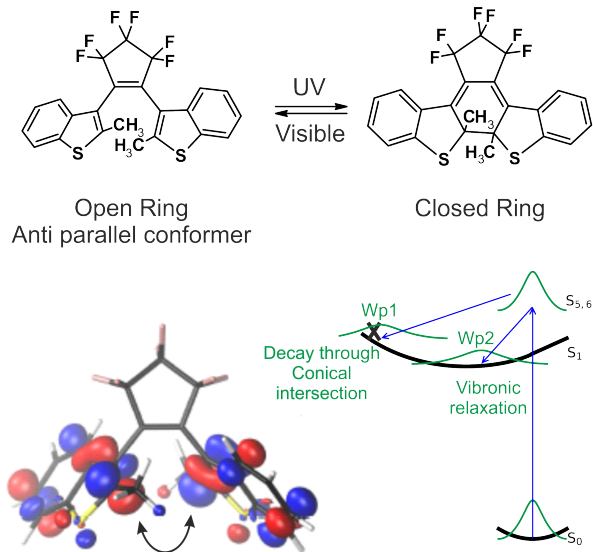


**Fig. 10** Top: scheme of the photochromic reaction of BTF6 (1,2-bis(2-methylbenzo[b]thiophen-3-yl)perfluorocyclopenten). Bottom left: LUMO+1 orbital calculated at the B3LYP/def2-TZVP level. Bottom right: scheme of the wavepacket movements. Work to be published in Ref. 171.

### 7.3 Dynamics of photochromic molecules.

The photoinduced dynamics of photochromic molecules is a vast field that has both a practical interest for industry and a fundamental interest given the variety of reaction mechanisms they exhibit. Here, it offers the opportunity to examine an opposite situation as that reviewed in the preceding section. The point here is how a weakly interacting reaction medium (argon cluster) affects a strong photoinduced dynamics in a guest molecule (a photochromic molecule) that undergoes a large intramolecular rearrangement. An interesting example is provided by the photodynamics of a normal

dithienylethene molecule: 1,2-bis(2-methylbenzo[b]thiophen-3-yl)perfluorocyclopentene (BTF6-C<sub>23</sub>H<sub>14</sub>F<sub>6</sub>S<sub>2</sub>). The open-ring isomer of this molecule has an antiparallel conformer, which, upon UV electronic excitation, makes a ring closure reaction. The latter is schemed in Fig. 10 together with a representation of the LUMO+1 orbital from which reaction proceeds. The double arrow underneath the orbital follows very simply the Woodward-Hoffmann rules to illustrate where the photocyclization proceeds. The reverse reaction can be photoinduced by visible light. The ring-closure (photocyclization)/ring-opening (photoreversion) sequence makes the photochromic property of BTF6. The photoinduced dynamics of the open-ring isomer of BTF6 was studied in situations where BTF6 is either fully free in a molecular beam or isolated within an argon cluster. This will be reported in a forthcoming article.<sup>171</sup> The experiment was performed in the real-time domain with a 80 femtosecond resolution. The molecule was pumped near 266 nm to the  $S_{5,6}$  states. This launched a wavepacket where several deformation modes of the molecule are excited. The latter fall in two categories, which make the initial wavepacket splitting very early in two part that evolve independently from each other. Each sub-wavepacket has its own dynamics. One (WP<sub>1</sub>) has an essentially ballistic movement and decays rapidly ( $\approx 0.5$  ps when BTF6 is free), through a conical intersection (CI). The other (WP<sub>2</sub>) is associated with a much slower process (3-10 ps for free BTF6), a vibronic relaxation within the excited potential energy surfaces. When BTF6 is isolated in an argon cluster, the splitting of the initial wavepacket into WP1 and WP2 still occurs. A dramatic effect is observed. WP<sub>1</sub> is strongly inhibited and most of the relaxation occurs from WP<sub>2</sub>. This is interpreted in Ref. 171 by the ballistic wavepacket "colliding" one or several argon repulsive walls. Then, it deviates significantly from reaching the CI.

To conclude this section, we point out that solvation of guest atoms or molecules by cluster hosts affects significantly the excited state dynamics of the guest. This was exemplified experimentally on atomic (Sec. 6) and non-reactive molecular (DABCO) guests. On the theoretical side, excited state dynamics of an atomic guest was actually coupled with the cluster degrees of freedom. The same task with a molecular guest, especially if it is less rigid than DABCO, would be a challenge essentially because the degrees of freedom, which control the geometry of the host, that of the guest and the guest-host arrangement likely evolve at order of magnitude different time scale.

## 8 Photoinduced bimolecular reactions on cluster

The crossed molecular beam technique is considered as a dedicated tool for studying the dynamics of elementary bimolecular reactions under the single collision regime. Historical achievement in this field can be found in the 1986 Nobel lectures of Herschbach and Lee.<sup>172,173</sup> The experimental insight given by this technique is an integration of the dynamics over the full reaction path from reactants to products. Attempts to explore reactions along the reaction path were initiated by Polanyi, the third 1986 Nobel laureate.<sup>174</sup> A breakthrough in this field was

the Transition-State spectroscopy technique (TS-Spec) pioneered in the group of Benoît Soep and applied to the  $\text{Hg} \cdots \text{Cl}_2$  reaction.<sup>52</sup> It consists in freezing the two reactants Hg and  $\text{Cl}_2$  in a 1:1 van der Waals complex and to promote the reaction by local optical excitation of Hg within the complex. The chemiluminescence of the  $\text{HgCl}^*$  product was monitored as a function of the frequency of the laser that turns on the reaction. The resulting action spectrum, more precisely the location and width of bands in the action spectrum deserved a spectroscopic information on the transition state of the reaction.

The present section addresses photoinduced reactions between reactant that are deposited on large, chemically inert clusters. The experimental technique used for these studies is a transposition of the transition state spectroscopy (TS-Spec) technique that has just been recalled. The first example reported here is a comparison between the TS-Spec study of the  $\text{Ca} \cdots \text{HBr}$  reaction when the van der Waals complex is isolated in a molecular beam to a situation where the van der Waals complex is bound to a large argon cluster.

The group of Benoît Soep has pioneered the TS-Spec study of Calcium-Hydrogen Halide reactions.<sup>175–177</sup> For instance, the action spectrum reported in Ref. 176 for the  $\text{Ca} + \text{HBr}$  reaction is shown in the middle panel of Fig. 11. It was assigned to a local excitation of the calcium atom with the excited orbital either in  $A'$  or  $A''$  alignment with respect to the  $\text{Ca-HBr}$  plane. Importantly, the  $A''$  band exhibits a progression due to the bending of the complex, interpreted as a deformation mode that is perpendicular to the reaction coordinate. In the same work, the measured action spectrum was simulated successfully by propagating wavepackets on model potential energy surfaces that mimic a harpoon type reaction. This revealed that the access to transition state of the harpoon reaction is multidimensional and that the coupling between the covalent and ion pair surfaces is very dependent upon the  $\text{Ca-HBr}$  bending angle, a première at that date!

Briant *et al.* transposed the TS-Spec technique to study the same  $\text{Ca}^* + \text{HBr} \longrightarrow \text{CaBr}^* + \text{H}$  reaction as above, but with the Ca and HBr reactants deposited at the surface of a  $\text{Ar}_{\approx 2000}$  cluster using the pick-up technique.<sup>178</sup> A standard CICR is performed.<sup>37</sup> Accordingly, the average number of reactants deposited *per* cluster was varied systematically and, with the help of the Poisson statistics, the observed chemiluminescence signal could be assigned to the reaction of a single Ca atom with a single HBr molecule, both forming a 1:1  $\text{Ca} \cdots \text{HBr}$  complex at the surface of the argon cluster. The action spectrum measured by these authors is reproduced in the top panel of Fig. 11. The resemblance with that recorded from the free 1:1  $\text{Ca-HBr}$  complex (middle panel of the figure) is clear. Nevertheless differences exist. Their origin was discussed by Briant *et al.* on the ground of the simulated spectrum shown in the bottom panel of Fig. 11. Briant *et al.* concluded that the access to the transition state of the reaction is significantly affected, although not fully transformed by the presence of the argon cluster. In particular, a broad component is added to the action spectrum. It was interpreted as the excited 4p orbital of calcium pointing towards the cluster surface and forcing movements of the complex that cannot be achieved when the complex is free.

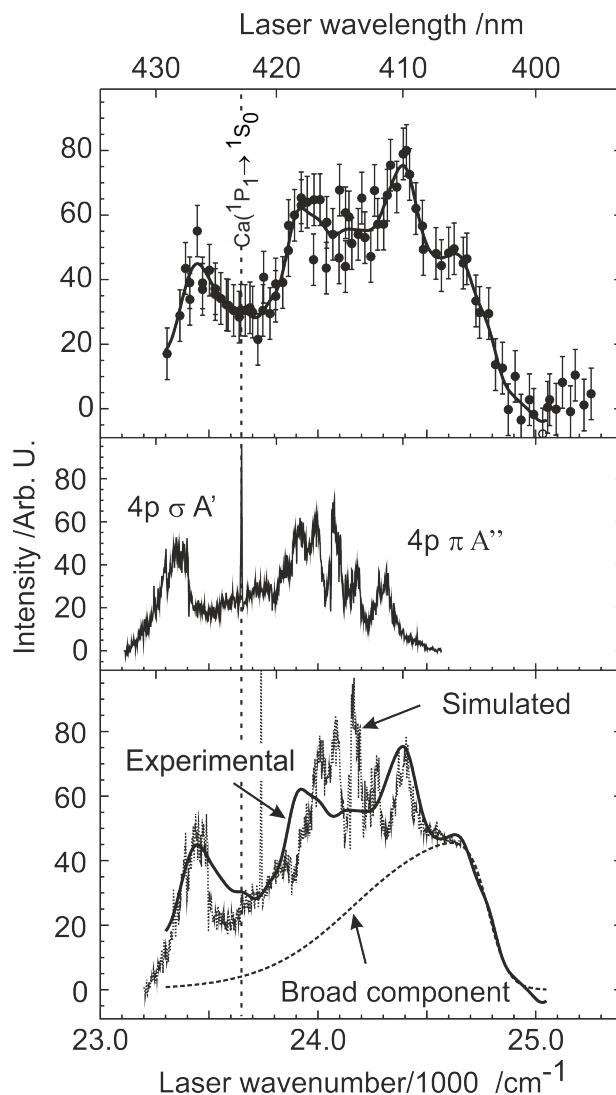


**Fig. 11** Top panel: Action spectrum of the  $1\text{Ca}^* + 1\text{HBr} \longrightarrow \text{CaBr}^* + \text{H}$  reaction on argon clusters ( $\text{Ar}_{\approx 2000}$ ). It was recorded by monitoring the  $\text{CaBr}^*$  chemiluminescence as a function of the wavelength of the laser that turns on the reaction. The solid line smoothes the experimental points. Middle panel: Action spectrum of the same reaction recorded in Ref. 176 for the free  $\text{Ca} \cdots \text{HBr}$  complex. Bottom panel: Comparison between the smoothed experimental data of the top panel and a simulation where the action spectrum in the middle panel is blue shifted by  $90\text{ cm}^{-1}$  and superimposed to the broad component shown as a dashed line in the figure. Reprinted from Ref. 178, with the permission of AIP Publishing.

The  $\text{Ca} + \text{CH}_3\text{F} \longrightarrow \text{CaF} + \text{CH}_3$  is another example of harpoon-like reaction where the access to the transition state of the reaction is multidimensional. No bound state of an extra electron exists indeed at the equilibrium geometry of  $\text{CH}_3\text{F}$  and the C–F has to be stretched for the molecule to attach an electron.<sup>179</sup> This creates a barrier which blocks the reaction in the ground electronic state and enables the 1:1  $\text{Ca} \cdots \text{FCH}_3$  complex to be stabilized.

Experiments were reported where the  $\text{Ca} + \text{CH}_3\text{F} \longrightarrow \text{CaF} + \text{CH}_3$  reaction was photoinduced in  $\text{Ca} \cdots \text{FCH}_3$  complexes, the latter being either free,<sup>180–182</sup> or deposited at the surface of an argon cluster.<sup>183</sup> These works included *ab-initio* calculations which associated a pseudopotential description of the  $[\text{Ca}^{2+}]$  and

[F<sup>7+</sup>] cores, a core polarization operator on calcium, an extensive Gaussian basis and a treatment of the electronic problem at the CCSD(T), MCSCF, RSPT2 and MRCI levels. The calculations of Refs. 180,182 documented excited potential energy surfaces on the dissociation side of the complex, when Ca + CH<sub>3</sub>F is formed. The calculations of Ref. 181 ran wavepackets over a 2D potential energy grid that described the Ca/CH<sub>3</sub>F assembly with a linear Ca – F – C backbone. The complete reaction coordinate going from Ca + CH<sub>3</sub>F to CaF + CH<sub>3</sub> was explored. The latter was defined as the difference between the Ca-F and F-C bond lengths (referred to the equilibrium geometry of the ground state Ca...FCH<sub>3</sub> complex). It goes from positive to negative when passing from the dissociative side Ca + CH<sub>3</sub>F of the complex to the reactive side where CaF + CH<sub>3</sub> is formed.

The calculation of Ref. 181 was successful to predict the absorption spectrum of the complex, which of course is sensitive essentially to the potential energy surfaces in the Franck-Condon region of excitation. It is however not fully realistic when considering the reaction coordinate all the way to the formation of CaF + CH<sub>3</sub>. Two other deformation coordinates are expected indeed to participate to the bond rearrangement: the ∠Ca – F – C bending angle to allow the formation of the strongly bound insertion intermediate FCaCH<sub>3</sub> and the CH<sub>3</sub> pyramidalization angle which switches from pyramidal in CH<sub>3</sub>F to planar when CH<sub>3</sub> is free.

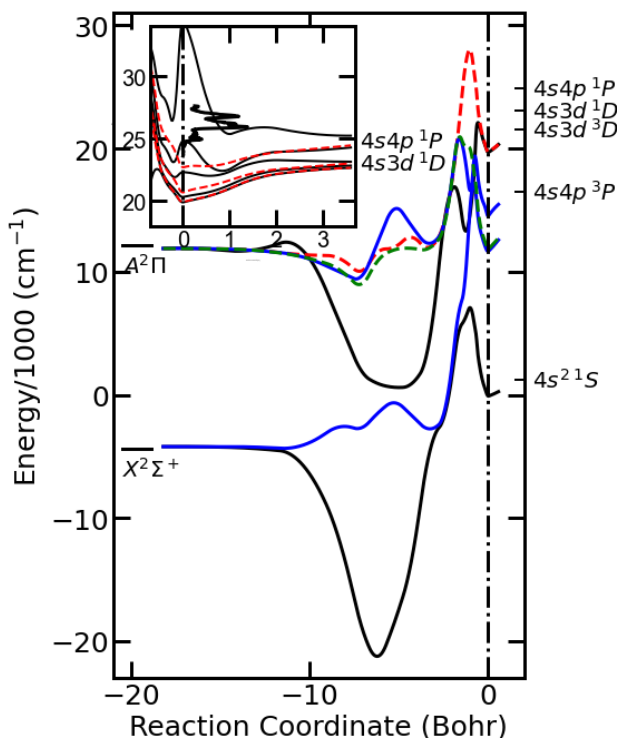


**Fig. 12** Calculated energies of the 1<sup>1</sup>A', 2<sup>1</sup>A' (solid black curves), 1<sup>1</sup>A'' (dashed red), 1<sup>3</sup>A', 2<sup>3</sup>A' (solid blue) and 1<sup>3</sup>A'' (dashed green) states along the reaction coordinate defined in the text (left: CaF + CH<sub>3</sub> products; right: Ca<sup>+</sup>CH<sub>3</sub>F reactants). The inset shows all the singlet curves correlating to the CH<sub>3</sub>F + Ca(4s3d<sup>1</sup>D, 4s4p<sup>1</sup>P) dissociation limit, together with the action spectrum reported in Ref. 183. Energies are given with respect to the Ca...FCH<sub>3</sub> well.

The present perspective article complements the calculations of Ref. 181. It includes the effect of adjusting the bending and pyramidalization angles mentioned above while scanning the reaction coordinate. These novel calculations, which keep the Ca/CH<sub>3</sub>F assembly with a C<sub>v</sub> symmetry, were conducted as follow. First, the F-C distance, and the ∠Ca – F – C angle were optimized for the ground electronic state at the MCSCF level while varying the Ca-F distance and keeping the CH<sub>3</sub> pyramidalization angle as in free CH<sub>3</sub>F. This defined an approximate reaction path. Then, a series of MRCI calculations were performed along this path for five pyramidalization angles of CH<sub>3</sub> between ∠F – C – H = 90° (planar geometry) and ∠F – C – H = 108.8° (equilibrium geometry in CH<sub>3</sub>F). Each MRCI calculation provided us with the energy of the 1<sup>1</sup>A', 2<sup>1</sup>A', 1<sup>1</sup>A'' singlet and 1<sup>3</sup>A', 2<sup>3</sup>A', 1<sup>3</sup>A'' triplet states as a function of the reaction coordinate for various values of the pyramidalization angle of CH<sub>3</sub>. For each state the lowest energy was retained when scanning the pyramidalization angle. The resulting energy curves are shown in the main part of Fig. 12. They are limited to those correlating to CaF(X<sup>2</sup>Σ<sup>+</sup>, A<sup>2</sup>Π) + CH<sub>3</sub> because of convergence troubles in the MRCI calculations. The numerous changes of the electron configuration along the reaction coordinate, successively Ca + FCH<sub>3</sub>, Ca...FCH<sub>3</sub>, Ca...F...CH<sub>3</sub>, Ca<sup>+</sup>...F<sup>-</sup>...CH<sub>3</sub>, F...Ca...CH<sub>3</sub> and CaF + CH<sub>3</sub> do not affect the excited states in the same way and the resulting root switching problems during the state and orbital optimization were difficult to handle. MRCI calculations, limited to Franck-Condon region of excitation, could be performed for a larger number of singlets states (up to 5<sup>1</sup>A' and 3<sup>1</sup>A''), i.e. state correlating up to Ca(4s4p<sup>1</sup>P) at infinite separation between Ca and CH<sub>3</sub>F (inset of Fig. 12).

Let us turn back to the transition-state spectroscopy work of Gaveau *et al.* who photoinduced the Ca + CH<sub>3</sub>F → CaF + CH<sub>3</sub> reaction in a Ca...CH<sub>3</sub>F complex deposited at the surface of an argon cluster.<sup>183</sup> The corresponding action spectrum is plotted against the calculated potential energy curves in the inset of Fig. 12. This shows that the excitation proceeded towards the manifold correlating to the Ca(4s4p<sup>1</sup>P) + CH<sub>3</sub>F dissociation. The spectrum does not look similar to that recalled in Fig. 11 for the Ca + HBr reaction. This was recognized in Ref. 183 and discussed as revealing a profound alteration of the Ca electronic structure. This is actually confirmed by the present calculation, especially when observing that the A' curves correlating to the Ca(4s4p<sup>1</sup>P) + CH<sub>3</sub>F dissociation. They are not parallel to the potential curves correlating to lower calcium states. These curves are actually strongly mixed with those correlating to Ca(4s5s<sup>1</sup>S) + CH<sub>3</sub>F. Fig. 12 reveals a complex landscape with several energy barriers and suspended wells on the ground and excited potential energy surfaces, that offer many coupling regions between the upper singlet molecular states that are populated by the laser excitation and lower singlet and triplet states.

Except the barrier on the 1<sup>1</sup>A' curve, all other barriers in Fig. 12 are lower than the 23,600 and 27,600 cm<sup>-1</sup> range of energies that is made available when the complex is excited within the action spectrum shown in the inset of the figure. The issue is important and reveals the key role played by the two extra angles (the CH<sub>3</sub> pyramidalization angle especially) that were considered to

built the potential curves in Fig. 12. Energy barriers above the  $27,600\text{ cm}^{-1}$  limit were indeed predicted along the singlet curves in the 2D potential calculation of Gloaguen *et al.*.<sup>181</sup> Accordingly, after Gloaguen *et al.* discussed the possibility of a tunneling reaction through the barrier in the  $2^1A'$  state, they suggested that the reaction could proceed along triplet energy curves after an intersystem crossing has occurred. The conclusion here is different. The energy curves reported in Fig. 12 were optimized along the  $\angle\text{Ca}-\text{F}-\text{C}$  bending angle and  $\text{CH}_3$  pyramidalization angle coordinates and show that the barrier in the  $2^1A'$  state is lowered below the excitation energy. The access to this barrier is likely sinusoidal and not easy to find, in agreement with the strongly structured action spectrum. Following Ref. 183, this structure can be thought as a vibrational progression due the  $\text{F}-\text{C}$  stretch mode.

The photoinduced  $\text{Ca} + \text{CH}_3\text{F} \longrightarrow \text{CaF} + \text{CH}_3$  reaction in  $\text{Ca}\cdots\text{FCH}_3$  complexes can be viewed as case study where the access to the transition state of the reaction is intrinsically multidimensional. It would therefore be informative to observe how the excitation of specific vibrational modes of the  $\text{CH}_3\text{F}$  moiety in the complex would promote or inhibit the reaction. This cannot be done when examining the band widths in the action spectrum of Ref. 183 because of the broadening due to argon. As well, this cannot be done on the free complex as in Refs. 180–182 because the internal temperature of the complex is fairly large and prevents a mode specific analysis of the action spectrum. Although certainly very difficult, this can probably be achieved when hosting  $\text{Ca}$  and  $\text{CH}_3\text{F}$  in a helium droplet to benefit of extremely narrow absorption band. In that case, an access would be given to mode specific excitation of the complex that would be extremely interesting to address in time resolved studies. Moreover, if hosting  $\text{Ca}\cdots\text{FCH}_3$  in helium droplet, an elegant way of documenting solvent effects in a stepwise manner would be picking-up extra atoms or molecules in the droplet. No such work has been tried yet.

## 9 Dynamics of multipartner processes hosted in clusters/nanodroplets

### 9.1 Hampered deformations of molecular complexes hosted in helium nanodroplets

Due to their superfluidity and weak interaction with guest molecules, Helium nanodroplet are often presented as a nearly ideal medium were to perform spectroscopic and dynamics studies.<sup>184</sup> Nevertheless, it is known for a long time that slow molecular rotations as that of  $\text{SF}_6$  are slowed down by the helium host, this being described phenomenologically by replacing gas phase rotational constants by much smaller effective constants.<sup>40</sup> A crude interpretation based on classical mechanics makes a link between smaller effective constants, *i.e.* larger moments of inertia and the fact that the rotating molecules drive a non-superfluid component into movement. Ref. 185 reviews a series of path-integral, variational, and diffusion quantum Monte Carlo calculations showing that within a purely quantum picture, the helium atoms of the non-superfluid component are not distinguishable from the other He atoms. Instead, they are dynamically exchanging with them. More recently, Lemeshko proposed that guest

molecules in helium nanodroplets could be described by angulars, *i.e.* pseudo-particles where a quantum rotor is dressed by the field of many-body excitations.<sup>186</sup>

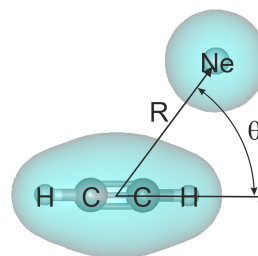


**Fig. 13** Electronic density of the  $\text{C}_2\text{H}_2\cdots\text{Ne}$  complex at the equilibrium geometry ( $R=3.95\text{ \AA}$  and  $\theta=43.3^\circ$ ). The coordinates  $R$  and  $\theta$  describe the large amplitude deformations of the complex. Reproduced from Ref. 187 with permission from the PCCP Owner Societies.

Regardless the picture, classical or quantum, a van der Waals bound molecular complex, *e.g.* the  $\text{C}_2\text{H}_2\cdots\text{Ne}$  complex shown in Fig. 13 is likely surrounded by a non-superfluid component when formed in a helium droplet. Large amplitude deformations of such complexes include a hindered rotation of the molecular moiety with respect to the van der Waals bond. The corresponding in-plane rotation of angular coordinate  $\theta$  is shown in Fig. 13. As the slow rotations that have just been reviewed, the hindered rotations in molecular complexes are likely perturbed by the non-superfluid component of the complex. With collaborators, we have explored this issue both experimentally and theoretically by considering  $\text{C}_2\text{H}_2\cdots\text{Ne}$ ,  $\text{Ar}$  and  $\text{Kr}$  complexes,<sup>187,188</sup>. The  $(\text{C}_2\text{H}_2)_2$  dimer has been studied also.<sup>189</sup>

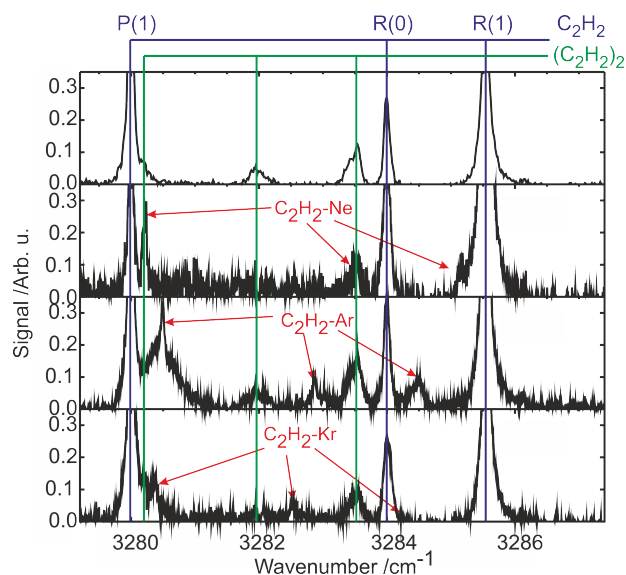


**Fig. 14** Spectra recorded in the  $\text{C}_2\text{H}_2$  (top panel) and  $\text{C}_2\text{H}_2\cdots\text{NeArKr}$  HENDI experiments of Refs. 187 and 188. Only the lower component of the  $\nu_3/\nu_2 + \nu_4 + \nu_5$  Fermi dyad is shown. The vertical lines label the rovibrational bands of  $\text{C}_2\text{H}_2$  (in blue) and  $(\text{C}_2\text{H}_2)_2$  (in green). Adapted from Refs. 187 and 188 with permission from the PCCP Owner Societies.

The experimental work in Refs. 187 and 188 was conducted along the well established HENDI technique.<sup>190</sup> Accordingly, (i)

helium droplets were generated by supersonic expansion (average size of a few thousands atoms). (ii) Rare gases (Ne, Ar, or Kr) and  $C_2H_2$  molecules were deposited sequentially on the droplets by pick-up and form the desired molecular complexes. (iii) The complex+droplet assemblies were illuminated by a tunable infrared laser. (iv) Finally, the flux of He-droplets, detected using a quadrupole mass spectrometer (tuned to the  $He_2^+$  mass), was monitored while scanning the laser across the  $\nu_3/\nu_2 + \nu_4 + \nu_5$  Fermi-type resonance of  $C_2H_2$ . The resulting HENDI spectrum informs on the absorption spectrum of the molecular complex within the droplet. HENDI spectra recorded for  $C_2H_2$ -Ne, Ar and Kr complexes are shown in Fig. 14 (bottom panels). For comparison, the  $C_2H_2$  HENDI spectrum recorded in Ref. 189 is shown in the top panel of the figure.

The red arrows in Fig. 14 indicate the spectral features that are associated with the  $C_2H_2 \cdots$  Rare gas complexes. The three features observed with  $C_2H_2 \cdots$  Ne retain attention since they are close to the P(1), R(0) and R(1) ro-vibrational transitions of  $C_2H_2$ , an indication that the rotation of  $C_2H_2$ , although constrained by the presence of Ne and by the helium environment, is close to be free. Three features are also observed with the two other  $C_2H_2 \cdots$  Rare gas complexes. Their shifts with respect to the P(1), R(0) and R(1) transitions of  $C_2H_2$  deviate from those of an almost free rotation. They are difficult to rationalize without a model treating both of the intrinsic dynamics of the complex and its perturbation by the helium environment. A numerical model was developed for this purpose in Ref. 188. It generalizes the concept of effective rotational constants and offers a phenomenological approach to the dynamical effect of the helium droplets on the large amplitude deformation, *i.e.* deformations along van der Waals modes of the hosted  $C_2H_2 \cdots$  Rare gas complexes.

Concerning the deformation dynamics of the complex along the weak van der Waals coordinates  $R$ ,  $\theta$  defined in Fig. 13, the model assumes that it is the same whether the  $C_2H_2$  moiety is in the ground vibrational state or excited to one of the components of the  $\nu_3/\nu_2 + \nu_4 + \nu_5$  Fermi dyad. Hence the bound states of  $C_2H_2 \cdots$  Rare gas complexes in one of these dyads are simply those of the ground state, shifted in the same amount,  $G_{LD}$  or  $G_{UD}$  whether the lower or the upper dyad is considered. The bound states in the ground vibrational states of the complex are provided by the *VRBoundScat* close-coupling program developed in the group of Jean-Michel Launay<sup>191–193</sup>. The  $C_2H_2$  moiety is represented as a pseudo rigid linear rotor with rotational and centrifugal correction constants  $B$  and  $D$ . It moves within the two dimensional  $C_2H_2 \cdots$  Rare gas potential energy surface  $V(R, \theta)$  where  $R$  and  $\theta$  are the van der Waals coordinates defined in Fig. 13. Of course, the *VRBoundScat* program acts in the 3D space and includes the overall rotation of the complex. The potential derived in the group of Jacky Liévin have been used in these calculations.<sup>194,195</sup>

The model treats the effect of the helium droplet phenomenologically by giving effective values to the constants  $B$  and  $D$  and to the reduced mass  $\mu$  of the  $C_2H_2 \cdots$  Rare gas complex, *i.e.* to the parameters that control the deformation of the complex ( $B$  and  $D$ ) and its overall rotation ( $\mu$ ). Then, the energy and oscillator strength of all the transitions from the ground state to the desired

component of Fermi dyad are calculated and each ground state level is weighted by its population at the droplet temperature. As a final step, the transitions are summed all together, hence simulating the absorption spectrum of the complex. To check the reliability of the model, the gas phase values of  $B$ ,  $D$  and  $\mu$  were used to simulate the spectrum of the free  $C_2H_2 \cdots$  Ar complex. It successfully reproduced that measured and simulated numerically by Bemish *et al.* using a different approach.<sup>196</sup>

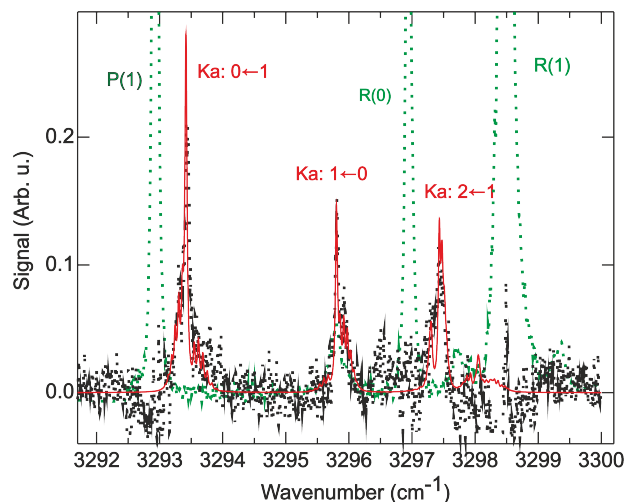


**Fig. 15** Comparison between the experimental (black dots) and simulated (red curve) spectra for the upper  $\nu_3/\nu_2 + \nu_4 + \nu_5$  Fermi dyad of the  $C_2H_2$ -Ar complex. The green dotted curve shows the acetylene-only signal which was subtracted to get the complex-only spectrum. The experimental and simulation data are taken from Ref. 188. The red labels consider the complex as a rigid asymmetric top molecule and the green ones the  $C_2H_2$  molecule as a free rotor.

After an appropriate adjustment of the  $B$ ,  $D$  and  $\mu$  parameters and of  $G_{LD}$  and  $G_{UD}$  dyad energies, the model accounts quantitatively for the experimental data in Fig. 14. An example is shown in Fig. 15. The adjusted parameters  $B$ ,  $D$ ,  $\mu$ ,  $G_{LD}$  and  $G_{UD}$  were discussed in Ref. 188. Two effects sensitively affect the observed spectra: the rigidity of the  $C_2H_2 \cdots$  Rare gas complex and the coupling dynamics between the complex and the non-superfluid and superfluid components of the nanodroplet. These two points are examined now.

*Rigidity of the  $C_2H_2$ -RG complex* - This information stems from the comparison between the map of energy levels calculated using the *VRBoundScat* program and the analytical expressions of Hutson which map the rotational states of a linear molecule perturbed by a rare gas atom through an anisotropic potential.<sup>197</sup> Two extreme situations are recognized by Hutson, whether the rotational constant of the molecule is much smaller or much larger than the anisotropy term of the potential. The  $C_2H_2 \cdots$  Ne complex enters in the first category and the  $C_2H_2$  moiety rotates almost freely. The  $C_2H_2 \cdots$  Ar and  $C_2H_2 \cdots$  Kr complexes fall between the two extremes and the rotation of  $C_2H_2$  is severely hindered.

*Coupling dynamics between the complex, the non-superfluid and the superfluid components of the nanodroplet* - Information about this coupling is brought by the fit parameters  $B$ ,  $D$  and  $\mu$  as ex-

tensively discussed in Ref. 188. Only the information brought by parameter B is recalled here. When a free  $C_2H_2 \cdots RG$  complex is described, B is taken to be the rotational constant of free  $C_2H_2$  ( $1.17 \text{ cm}^{-1}$ ). In helium nanodroplets, the best fit value of B is 1.04 for  $C_2H_2$  and it is 1.14, 1.09 and  $1.09 \text{ cm}^{-1}$  for the  $C_2H_2 \cdots Ne$ ,  $C_2H_2 \cdots Ar$  and  $C_2H_2 \cdots Kr$  complexes, respectively. This was interpreted as a competition between the formation of a non-superfluid shell about either  $C_2H_2$  or the  $C_2H_2 \cdots RG$  complex and a repelling effect of the rare gas atom on the non-superfluid component of the nanodroplet, which is pushed away from the rotating  $C_2H_2$  molecule.

The model that has just been recalled treats the rovibrational structure of  $C_2H_2 \cdots RG$  complexes quantum mechanically. However, it bypaths two difficulties. One is technical. The same effective rotational constant B was used to treat of helium droplet effect on the two molecular rotations: the in-plane rotation represented in Fig.13 and the out-of-plane rotation, which corresponds actually to an overall rotation of the complex. For a weakly bond complex as  $C_2H_2 \cdots Ne$ , this is fully justified because the helium droplet likely affects the two rotations in about the same way. This might not be the case for more rigid complexes as  $C_2H_2 \cdots Kr$ . The second difficulty is that the model bypaths the quantum character of the helium nanodroplet. The latter show up very indirectly by observing that the D parameter is four order of magnitude larger in helium nanodroplet than in the gas phase, an indication that collective excitation of the nanodroplet is strongly coupled with the molecular rotation.<sup>198,199</sup> We consider that the body of results that has just been reviewed is sufficiently solid to stimulate theoretical works where this double quantum character is included explicitly. A promising direction is the hybrid quantum method developed by Vilà *et al.* that combines time dependent density functional theory for describing the helium nanodroplet) and quantum dynamics to describe the molecule. This method has been used recently to model rotational and vibrational energy relaxation in a diatomic molecule hosted in a helium droplet.<sup>201,202</sup>

## 9.2 A non-statistical multi-member $Ca/N_2O$ chemiluminescent reaction within argon clusters and helium nanodroplets

**A historical perspective on the  $Ca/N_2O$  system** - Gas phase reactions of metal atoms with oxidant molecules have attracted a considerable interest in the 1970's and 1980's.<sup>203,204</sup> A particular attention was given to chemiluminescent reactions of alkaline earth atoms as candidates to design chemical lasers. Renewed interest came when the addition of metals to combustion systems was proposed to reduce emissions of  $N_2O$ , a greenhouse gas.<sup>205</sup> For example, Gao *et al.* proposed that a porous medium made with calcium decorated fullerene ( $Ca-C_{60}$ ), could be efficient to capture and transform  $N_2O$  chemically.<sup>206</sup>

Metal atom/ $N_2O$  reactions are also interesting from a pure physical chemistry point of view. It is driven by an electron transfer from the metal to  $N_2O$ , but undistorted  $N_2O$  has a negative electron affinity (the controversial electron affinity of  $N_2O$  is extensively reviewed in Ref. 207). Hence, as met above with the

$Ca + HBr$  and  $Ca + CH_3F$  reactions, at least two coordinates are at play in the entrance channel of the reaction. Actually, the  $Ca + N_2O$  reaction appears as paradigm of non-Arrhenius reactions where several reaction pathways associated with different activation energies compete with each other.<sup>208-210</sup>

The chemiluminescent reaction of  $Ca + N_2O$  forming  $CaO$  was first reported by Zare and coworkers.<sup>211,212</sup> Further investigations were performed by Dagdigian and coworkers under a beam-gas arrangement with Ca in ground state  $4s^2 \ ^1S_0$  or in metastable states  $4s4p \ ^3P_0$  and  $4s3d \ ^1D$ .<sup>213,214</sup> Numerous spectroscopy techniques, including laser-induced fluorescence, resolved fluorescence, optical-optical double resonance techniques, sub-Doppler Intermodulation, Fourier transform were used to assign thousands of  $CaO$  lines and provide reliable spectroscopic constants of  $CaO$  electronic states.<sup>215-221</sup> This motivated recent ab-initio calculations by Céline Léonard and coworkers, limited however to low lying states of  $CaO$ .<sup>222-224</sup> In spite of this intense experimental and computational activity, the complex spectroscopy of  $CaO$  within the orange and green bands is still not fully unraveled.

**Motivation for new HENDI-like and CICR experiments on the  $Ca/N_2O$  system** - Most experiments recalled above where  $Ca + N_2O$  chemiluminescence was reported were performed under a multicollision regime and imply a complex reaction mechanism. Reaction between single reactants  $Ca$  and  $N_2O$  does not provide indeed enough energy to excite the chemiluminescence which is observed. We speculate that a multicentre transition state, where several  $Ca$  atoms and  $N_2O$  molecules interact, is at play. We found useful to check this anticipation here. CICR (deposition for the reactants on argon clusters) and HENDI-like (deposition on helium droplets) experiments were performed for this purpose on the  $Ca + N_2O$  chemiluminescent reaction. Finite size reaction media formed by argon clusters or helium droplets offer control on the number of deposited reactants and therefore inform on the stoichiometry of the reaction which is observed.<sup>37,66,178</sup>

**Experimental** - The setup used for CICR experiments is described in Ref. 225. The same setup was adapted to HENDI-like experiments as described in Ref. 226. A beam carrying either argon clusters ( $Ar_{\approx 2000}$ ) or helium nanodroplets ( $He_{\approx 20000}$ ) crosses two pickup regions and capture collisionally  $Ca$  atoms and  $N_2O$  molecules. The resulting chemiluminescence is collected after the pick-up regions. After dispersion in a monochromator, it is recorded by a photomultiplier with cut-off at 900 nm. Spectra below are corrected for transmission and response of the optical chain.

An important issue in this work was to determine how many  $Ca$  atoms and how many  $N_2O$  molecules must be present on the same cluster (or droplet) for observing chemiluminescence. Two series of HENDI-like experiments were conducted separately where the average number of calcium atoms ( $\langle n_{Ca} \rangle$ ) and that of  $N_2O$  molecules ( $\langle n_{N_2O} \rangle$ ) *per* droplet were varied systematically. For  $\langle n_{Ca} \rangle$ , the temperature  $T_{Ca}$  of the crucible, where solid calcium was evaporated, was adjusted. A calibration curve was necessary to relate  $T_{Ca}$  and  $\langle n_{Ca} \rangle$ . This was achieved by recording a laser induced fluorescence (LIF) signal  $Ca(^1P_0 \rightarrow ^1S)$  as a function of

$T_{Ca}$  on the same set up, with no  $N_2O$  molecule present on the droplets. The LIF signal followed a first order Poisson law since calcium dimers and larger multimers do not absorb or emit at the same wavelength as the atom. This allowed for scaling  $T_{Ca}$  with  $\langle n_{Ca} \rangle$ . However, the helium droplets are light and fragile and their flux, which was measured using a mass spectrometer on the beam axis, decreased as  $\langle n_{Ca} \rangle$  was increased. This was compensated while constructing the calibration curve. The average number  $\langle n_{N_2O} \rangle$  was varied by adjusting the pressure in the foreline of the pick-up. The  $N_2O$  pressure in the pick-up region was monitored by measuring the pressure in the chamber which hosts the pick-up region. These pressures are proportional to each other and also proportional to  $\langle n_{N_2O} \rangle$ . No calibration curve is needed in this case.

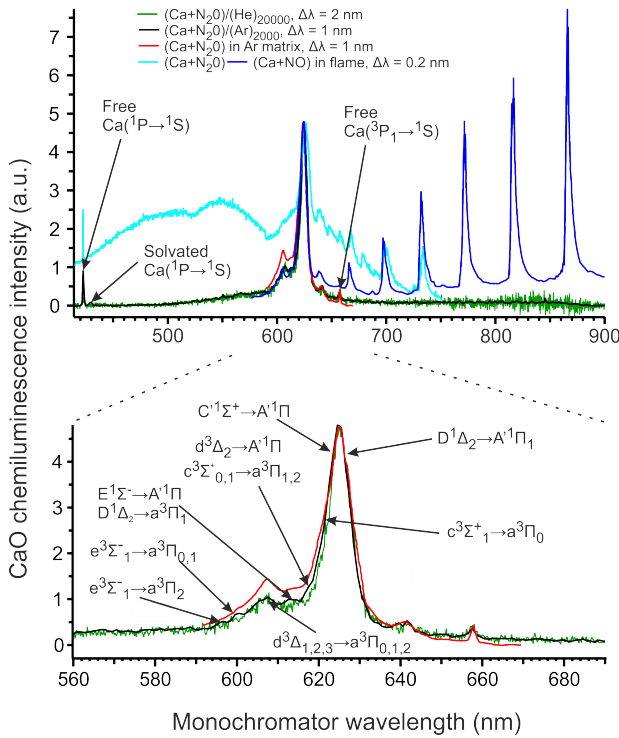


**Fig. 16** Chemiluminescence spectra recorded from  $Ca/N_2O$  mixtures deposited on helium nanodroplets (green curve;  $He_{\approx 20000}$ ) and argon clusters (black curve;  $Ar_{\approx 2000}$ ), normalized at their maximum. The bottom panel magnifies the wavelength scale. For comparison, the top panel includes chemiluminescence spectra recorded during co-deposition of a  $Ca/N_2O/Ar$  mixture on a cold plate (red curve; Ref. 219), in flame carrying  $Ca/N_2O$  (cyan curve) or  $Ca/NO$  (blue curve)<sup>227</sup>. Observed Ca transitions are labeled in the top panel. Known transitions of  $CaO$  are located in the bottom panel.<sup>216–219,221</sup>

**Chemiluminescence spectra and stoichiometry** - The chemiluminescence observed from  $Ca/N_2O$  mixtures deposited on helium nanodroplets (green curve) and argon clusters (black curve) are reported in the top panel of Fig. 16, their horizontal scale being magnified in the bottom panel. Strikingly, the two spectra, which are fairly structured, are identical within experimen-

tal noise. In particular no wavelength shift is observed between them. This suggests that the fluorescence emitter,  $CaO$  as discussed below, is free and has the same electronic and vibrational internal energy distribution in both experiments. If not free indeed, energy relaxation and wavelength shift should be different between the two experiments because solvation of  $CaO$  on argon clusters is certainly more invasive than solvation in helium droplets as observed with  $BaO$  in various cluster environments.<sup>48,228</sup> From this point of view, the similarity between the present two spectra and that recorded in the matrix experiment of Ref. 219 (red curve in the top panel of Fig. 16) is surprising at a first glance. However, this is not unexpected given the experimental conditions in Ref. 219. Chemiluminescence could be observed only during codeposition of  $Ca/N_2O/Ar$  onto the cold plate where the matrix was grown. Hence, the reaction may take place at the surface of the growing argon matrix with the  $CaO$  product emitting chemiluminescence before included into the matrix. In a sense, the matrix experiment of Ref. 219 and the present experiment on argon clusters mimic each other. Given the similarity between the three chemiluminescence spectra which have just been discussed, a similar reaction mechanism is at play in these experiments where a reaction medium (helium droplet, argon cluster or argon surface) is present. As will appear below, a different scenario is encountered when the  $Ca/N_2O$  chemiluminescence is observed in flame and beam-gas experiments where no such reaction medium is present.

A series of spectra were recorded in helium droplets as a function of  $\langle n_{Ca} \rangle$  and  $\langle n_{N_2O} \rangle$ . After summing each spectrum over the fluorescence wavelength, the total chemiluminescence signal was obtained. It is shown in Fig. 17 as a function of  $\langle n_{Ca} \rangle$  (left panel) and  $\langle n_{N_2O} \rangle$  (right panel). Linear combinations of Poisson distributions of order  $k$  ( $P_k(\langle n \rangle) = \frac{\langle n \rangle^k}{k!} \exp^{-\langle n \rangle}$ ) are shown also. The best agreement with experiment is found with  $1-P_1(\langle n_{Ca} \rangle)-P_2(\langle n_{Ca} \rangle)$  and  $1-P_1(\langle n_{N_2O} \rangle)$ , telling that the observed chemiluminescence is due to clusters carrying 3 or more Ca atoms and 2 or more  $N_2O$  molecules. These values correct a preliminary report of this stoichiometry in Ref. 229.

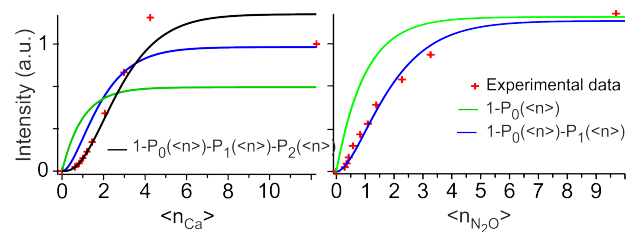


**Fig. 17** Total chemiluminescence signal as a function of the average number of Ca atoms (left panel) and  $N_2O$  molecules (right panel) per cluster. The experimental data (red crosses) are fitted by appropriate linear combination of Poisson distributions (solid curves). To appreciate the sensitivity to this choice, several combinations of Poisson distributions are shown in the figure.

**Reaction mechanism in presence of a reaction medium** - Relevant energetics of the  $Ca/N_2O$  system are listed in Tab. 1. The electronic transitions shown in Fig. 16 indicate that  $CaO$  levels up to  $e^3\Sigma^-$  (3.1 eV electronic energy) and Ca levels up to  $4s4p^1P$

Ca		Term Energy (eV)	Refs.		
	$4s^2^1S$	0			
	$4s4p^3P$	1.89		230	
	$3d4s^3D$	2.52		230	
	$3d4s^1D$	2.71		230	
	$4s4p^1P$	2.93		230	
CaO	$T_{00}$ (eV)	Refs.	CaO	$T_{00}$ (eV)	Refs.
$X^1\Sigma^+$	0				
$a^3\Pi_i$	1.03	216–218	$A'^1\Pi$	1.07	216–218
$b^3\Sigma^+$	1.18	231	$A^1\Sigma^+$	1.43	221
$c^3\Sigma^+$	3.03	232	$D^1\Delta$	3.047	232
$d^3\Delta$	3.07	232	$C'^1\Sigma^+$	3.054	233
$e^3\Sigma^-$	3.1	232	$E^1\Sigma^-$	3.09	232
Reactions			$\Delta H$ (eV)		Refs.
$\text{Ca} + \text{Ca} \longrightarrow \text{Ca}_2$			-0.13		234
$\text{Ca} + \text{N}_2\text{O} \longrightarrow \text{CaO} + \text{N}_2$			-2.62		$D_{\text{Ca-O}}$ <sup>235</sup>
$\text{Ca}_2 + 2\text{N}_2\text{O} \longrightarrow 2\text{CaO} + 2\text{N}_2$			-5.11		$D_{\text{N}_2-\text{O}}$ <sup>236</sup>
$\text{Ca}_3 + 2\text{N}_2\text{O} \longrightarrow 2\text{CaO} + 2\text{N}_2 + \text{Ca}$			-4.77		$D_{\text{Ca}_3}$ <sup>237</sup>

**Table 1** Relevant energetics for the Ca/N<sub>2</sub>O system.

(2.93 eV) are populated. Such large energies exceed that produced by a single  $\text{Ca} + \text{N}_2\text{O} \longrightarrow \text{CaO} + \text{N}_2$  reaction (2.62 eV), a situation which is in line with the observation that at least three calcium atoms and at least two N<sub>2</sub>O molecules produce the observed fluorescence. The reaction  $\text{Ca}_3 + 2\text{N}_2\text{O} \longrightarrow 2\text{CaO} + 2\text{N}_2 + \text{Ca}$  is exoergic by 4.77 eV (see Tab. 1), enough to account for the observed chemiluminescence signals.

The following picture emerges. The reaction medium, helium nanodroplet or argon cluster (even an argon surface as in Ref. 219) puts the reactants in interaction with each other and acts as a thermal bath to stabilize a complex made with at least 3 Ca atoms and 2 N<sub>2</sub>O molecules, enroute towards a five member (or more) transition state. At this initial step, a strong coupling exists between the reaction medium, the internal degrees of freedom of the reactants and movement along the reaction coordinate. Accordingly, the reaction is initiated at the reaction medium temperature. Given the very low temperature of helium droplets (0.38 K), we can state that the access to the transition state of the reaction is essentially barrierless. Beyond the transition state when the bond rearrangement starts, a large excess energy is released and hot products (*e.g.* CaO) are formed. Strong rapid intra- and inter-molecular movements are excited. Their evolution time is likely much shorter than the response time of the reaction medium, which therefore decouples from them. Accordingly, the internal energy of the reaction products weakly relax towards the reaction medium and essentially reflect the reaction dynamics across the transition state.

To complete the discussion on the transition state, it is interesting to mention the density functional theory (DFT) calculations of Gao *et al.* on Ca/N<sub>2</sub>O/C<sub>60</sub> clusters.<sup>206</sup> A strong out-of-linearity distortion of the N<sub>2</sub>O molecule is observed when one or two N<sub>2</sub>O molecules interact with a single Ca atom at the surface of C<sub>60</sub>. A significant barrier of 0.032 eV (0.045 eV when two molecules are present) prevents the N<sub>2</sub>O molecules to be dissociated as N<sub>2</sub> + O in the CaC<sub>60</sub> environment. Although the analogy with the present work must be handled with care, we notice that non-linear N<sub>2</sub>O

has a positive electron affinity, hence favoring an electron transfer and making it barrierless when additional Ca atoms and N<sub>2</sub>O molecules are present.

**Comparison with situations where no reaction medium is present** - Irvin and Dagdigian conducted experiments in a beam-gas configuration.<sup>214</sup> Calcium atoms, which were carried by the beam, have always a low density. In contrast, N<sub>2</sub>O was added to the gas up to high density. Hence, experimental conditions can be varied from single Ca + N<sub>2</sub>O collisions to a multicolision regime where a single calcium atom was colliding several N<sub>2</sub>O molecules and upon reaction, the reaction product could be further collided by N<sub>2</sub>O molecules. The chemiluminescence spectrum recorded under the single collision regime was assigned to CaO( $A'^1\Pi \rightarrow X^1\Sigma^+$ ) emission. No similarity with this spectrum can be recognized in the spectra recorded in the present work. This suggests that the  $1\text{Ca} + 1\text{N}_2\text{O} \longrightarrow \text{CaO} + \text{N}_2$  reaction has a barrier that is overcome in beam-gas collisions and not under the very small collision energies that prevail in the present droplet/cluster experiments. This fits with the work of Futerko and Fontijn where an activation barrier for forming CaO( $a^3\Pi_i$ ) is calculated to 0.033 eV and evaluated to 0.057 eV after reexamination of the experimental work of Ref. 208. Importantly, no other chemiluminescence than CaO( $A'^1\Pi \rightarrow X^1\Sigma^+$ ) was observed by Irvin and Dagdigian under the multicolision regime, suggesting that further exothermic reaction  $\text{CaO}^* + \text{N}_2\text{O} \longrightarrow \text{CaO}_2^* + \text{N}_2$  documented in Ref. 239 is not at play when a single Ca atom is present.

A multicolision regime, where several Ca atoms and several N<sub>2</sub>O (or NO) molecules are present, is achieved in flame experiments performed by Capelle *et al.* a long time ago.<sup>227</sup> The corresponding spectra (cyan and blue curves) are compared in Fig. 16 with those recorded here (green and black curves) and that recorded in matrix (red curve). Although similarities can be recognized, these spectra differ significantly from those already discussed. Only the blue side of the Ca/NO spectrum reproduces the spectra of the present work, whereas its red side exhibits a long progression assigned to the CaO( $A'^1\Pi \rightarrow X^1\Sigma^+$ ) transition, which is close to that recalled above from Ref. 214. The Ca/N<sub>2</sub>O spectrum of Ref. 227 mimics our spectra only in its red side, otherwise it has a large extension to the blue that does not exist in the present spectra. The difference between the Ca/NO and Ca/N<sub>2</sub>O spectra fits with the fact that reactions forming CaO in Ca/NO mixtures are less exoergic and therefore the available energy to excite CaO is smaller than in Ca/N<sub>2</sub>O mixtures.

As seen above, significant differences exist between pure gas phase flame spectra and the very similar three spectra where a reaction medium is present. This suggests a very different reaction mechanism in the flame experiments. A chain of elementary processes including energy pulling within the reaction products is more likely at play in these experiments than access to a complex transition state as encountered here when a reaction medium is present.

**Perspectives** No full simulation of the observed chemiluminescence is provided in Fig. 16 to allow a definitive assignment of the observed CaO transitions. Such simulation has actually been

tried, unsuccessfully, using the known CaO energy levels listed in Tab. 1. In particular, the most intense chemiluminescence peak could not be fully accounted by the sole  $\text{CaO}(C^1\Sigma^+ \rightarrow A^1\Pi)$  and  $\text{CaO}(D^1\Delta \rightarrow A^1\Pi)$  transitions. This may be due to large vibrational and rotational excitation of CaO which forces using spectroscopic constants outside their validity range. Alternatively, yet poorly documented states of CaO of large electronic energy may contribute to the chemiluminescence in this energy region. Qualitative information on such states is provided by *ab-initio* calculations in the group of Céline Léonard, which otherwise are devoted to predictions of almost spectroscopic quality on the low lying states of CaO.<sup>222,223</sup> A special attention should be given to the assignment of the 640 nm band, which is especially visible in the bottom panel of figure 16. It appears also in the top panel of the figure and seems shifted with respect to the  $\Delta v = 6$  band of the  $A^1\Sigma^+, v' \rightarrow X^1\Sigma^+, v''$  vibrational progression (see blue curve recorded in the Ca+ NO flame experiment). We consider this band as unassigned since it is unlikely associated with vibrationally excited  $A^1\Sigma^+$  state, even if a severe population inversion is present. Finally, emission of the calcium superoxide  $\text{CaO}_2$  must be considered also. A multistep reaction forming  $\text{CaO}_2$  in a Ca/ $\text{N}_2\text{O}$  vapor has been reported indeed.<sup>239</sup>

It seems difficult to imagine information on the yet poorly (or even unassigned) CaO transitions from experimental spectroscopy only. The latter fall indeed in very congested spectral region where very broad bands associated with  $\text{CaO}_2$  molecule may also be present. A better option would be deriving spectral information on CaO from high level *ab initio* calculations in the spirit as those reported above from the groups of Céline Léonard. This will be a very interesting challenge from a strictly theoretical point-of-view given the high electronic and vibrational energy contained in the CaO molecule. Tracking the multi-centre transition state within a strongly multi-configurational and multi-dimensional landscape would be another theoretical challenge. Very efficient optimization methodologies as those described in Refs. 240–243 still have to include the multi-configurational character of the interaction, with the difficulty that it is extremely geometry dependent near the transition state of the reaction.

## 10 Summary and perspectives

The present perspective article has reviewed a series of works that examine how structural and electronic relaxation is affected by the presence of an environment. These studies were conducted in finite size rare gas clusters and helium droplets rather than in macroscopic condensed media. This offers the advantage that diagnostics originally developed for reaction dynamics in the gas phase (e.g. time-resolved photoelectron spectroscopy, depletion spectroscopy) can be used. They offer extremely detailed experimental information on the structure and energy state of the detected species, which form a solid basis to develop state-of-the-art theoretical approaches, also reviewed here. The complementarity between experimental and theoretical information is a characteristic of this research field.

A lot of the works that are reviewed here address the response of a host-guest assembly to electronic excitation. The intrinsic response of the host (rare gas cluster or helium droplet) and

unimolecular processes within the guest (atom or molecules) are documented, essentially. Only a very limited body of information concerns bi- and multi-molecular processes. In the perspective where the host-guest studies is a way to approach reaction dynamics in solvent it would be very useful to develop the latter research direction. An elegant way to proceed would be to pick-up reactant molecules (A and B) and solvent molecules (S) in a helium droplet, to turn on a reaction between A and B (electronic or vibrational excitation of the reactants) and observe its dynamics as a function of the number of solvent molecules, using state-of-the-art experimental approaches such as real-time measurements with full characterization of the structure and quantum state of the detected species.

## Acknowledgments

Helpful discussion with Claudine Crépin (ISMO, Orsay, France) and Nadine Halberstadt (LCAR, IRSAMC, Toulouse, France) are acknowledged.

## Notes and references

- 1 J. Jortner, in *Analysis and Control of Ultrafast Photoinduced Reactions*, ed. O. Kühn and L. Wöste, Springer Berlin Heidelberg, Berlin, Heidelberg, 2007, pp. 1–23.
- 2 K. F. Bonhoeffer and L. Farkas, *Z. Phys. Chem.*, 1928, **134**, 337–344.
- 3 R. D. Levine, *Molecular Reaction Dynamics*, Cambridge University Press, Cambridge, 2005.
- 4 J. Elm, J. Kubecka, V. Besel, M. J. Jääskeläinen, R. Halonen, T. Kurtén and H. Vehkamäki, *Journal of Aerosol Science*, 2020, **149**, 105621.
- 5 J. N. Smith, D. C. Draper, S. Chee, M. Dam, H. Glicker, D. Myers, A. E. Thomas, M. J. Lawler and N. Myllys, *J. Aerosol Sci.*, 2021, **153**, 105733.
- 6 M. Fárnik, J. Fedor, J. Kočíšek, J. Lengyel, E. Pluhařová, V. Poterya and A. Pysanenko, *Phys. Chem. Chem. Phys.*, 2021, **23**, 3195–3213.
- 7 H. Haberland, *Clusters of Atoms and Molecules I*, Springer Verlag, Berlin, 1993.
- 8 H. Haberland, *Clusters of Atoms and Molecules II*, Springer Verlag, Berlin, 1994.
- 9 R. Johnston, *Atomic and Molecular Clusters*, CRC Press, 1st edn., 2002.
- 10 J. Jortner, R. D. Levine and S. A. Rice, *Adv. Chem. Phys.*, 1988, **70**, 1–34.
- 11 S. Goyal, D. L. Schutt and G. Scoles, *Acc. Chem. Res.*, 1993, **26**, 123–130.
- 12 A. W. Castleman, Jr. and K. H. Bowen, Jr., *J. Phys. Chem.*, 1996, **100**, 12911–12944.
- 13 Z. Bačić and R. E. Miller, *J. Phys. Chem.*, 1996, **100**, 12945–12959.
- 14 L. S. Bartell, *Annu. Rev. Phys. Chem.*, 1998, **49**, 43–72.
- 15 C. Bostedt, T. Gorkhover, D. Rupp and T. Möller, in *Clusters and Nanocrystals*, ed. E. Jaeschke, S. Khan, J. R. Schneider and J. B. Hastings, Springer International Publishing, Cham, 2019, pp. 1–49.

- 16 G. Scoles, *The Chemical Physics of Atomic and Molecular Clusters*, North-Holland, Amsterdam, 1990.
- 17 J. Jortner, *Z. Phys. D*, 1992, **24**, 247–275.
- 18 J. Jortner, *J. Chim. Phys.*, 1995, **92**, 205.
- 19 B. Hartke, *Angew. Chem. Int. Ed.*, 2002, **41**, 1468–1487.
- 20 R. S. Berry and B. M. Smirnov, *Comput. Theor. Chem.*, 2013, **1021**, 2–6.
- 21 F. Baletto and R. Ferrando, *Rev. Mod. Phys.*, 2005, **77**, 371–423.
- 22 C. Reichardt and T. Welton, in *Solvents and Solvent Effects in Organic Chemistry*, Wiley-VCH, Weinheim, 4th edn., 2011, pp. 359–508.
- 23 S. Leutwyler and J. Bosiger, *Faraday Discuss.*, 1988, **86**, 225–240.
- 24 S. Leutwyler and J. Bosiger, *Chem. Rev.*, 1990, **90**, 489–507.
- 25 M. Schmidt, M. Mons and J. Lecalvé, *Chem. Phys. Lett.*, 1991, **177**, 371–379.
- 26 D. Sicinska, P. Paneth and D. G. Truhlar, *J. Phys. Chem. B*, 2002, **106**, 2708–2713.
- 27 A. C. Plenert, E. Mendez-Vega and W. Sander, *J. Am. Chem. Soc.*, 2021, **143**, 13156–13166.
- 28 M. Hochlaf, *Phys. Chem. Chem. Phys.*, 2017, **19**, 21236–21261.
- 29 M. Ahmed and O. Kostko, *Phys. Chem. Chem. Phys.*, 2020, **22**, 2713–2737.
- 30 W. E. Ernst and A. W. Hauser, *Phys. Chem. Chem. Phys.*, 2021, **23**, 7553–7574.
- 31 M. Mudrich, A. C. LaForge, A. Ciavardini, P. O’Keeffe, C. Callegari, M. Coreno, A. Demidovich, M. Devetta, M. D. Fraia, M. Drabbels, P. Finetti, O. Gessner, C. Grazioli, A. Hernando, D. M. Neumark, Y. Ovcharenko, P. Piseri, O. Plekan, K. C. Prince, R. Richter, M. P. Ziemkiewicz, T. Möller, J. Eloranta, M. Pi, M. Barranco and F. Stienkemeier, *Nat. Commun.*, 2020, **11**, 112.
- 32 E. R. Bernstein, *J. Phys. Chem.*, 1992, **96**, 10105–10115.
- 33 E. R. Bernstein, K. Law and M. Schauer, *J. Chem. Phys.*, 1984, **80**, 207–220.
- 34 H. P. Kaukonen, U. Landman and C. L. Cleveland, *J. Chem. Phys.*, 1991, **95**, 4997–5013.
- 35 T. E. Gough, M. Mengel, P. A. Rowntree and G. Scoles, *J. Chem. Phys.*, 1985, **83**, 4958.
- 36 A. Lallement, J. Cuvellier, J.-M. Mestdagh, P. Meynadier, P. de Pujo, O. Sublemontier, J. P. Visticot, J. Berlande and X. Biquard, *Chem. Phys. Lett.*, 1992, **189**, 182.
- 37 J.-M. Mestdagh, M.-A. Gaveau, C. Gée, O. Sublemontier and J. P. Visticot, *Int. Rev. Phys. Chem.*, 1997, **16**, 215–247.
- 38 S. Goyal, D. L. Schutt and G. Scoles, *Phys. Rev. Lett.*, 1992, **69**, 933–936.
- 39 S. Goyal, D. L. Schutt and G. Scoles, *J. Phys. Chem.*, 1993, **97**, 2236–2245.
- 40 M. Hartmann, R. E. Miller, J. P. Toennies and A. Vilesov, *Phys. Rev. Lett.*, 1995, **75**, 1566–1569.
- 41 S. Grebenev, J. P. Toennies and A. F. Vilesov, *Science*, 1998, **279**, 2083–2086.
- 42 J. P. Toennies and A. F. Vilesov, *Annu. Rev. Phys. Chem.*, 1998, **49**, 1–41.
- 43 F. Stienkemeier, J. Higgins, W. E. Ernst and G. Scoles, *Phys. Rev. Lett.*, 1995, **74**, 3592–3595.
- 44 F. Stienkemeier, J. Higgins, W. E. Ernst and G. Scoles, *Z. Phys. B*, 1995, **98**, 413–416.
- 45 F. Stienkemeier, W. E. Ernst, J. Higgins and G. Scoles, *J. Chem. Phys.*, 1995, **102**, 615–617.
- 46 J. Higgins, C. Callegari, J. Reho, F. Stienkemeier, W. E. Ernst, M. Gutowski and G. Scoles, *J. Phys. Chem. A*, 1998, **102**, 4952–4965.
- 47 J. P. Toennies and A. F. Vilesov, *Angew. Chem. Int. Ed.*, 2004, **43**, 2622–2648.
- 48 E. Lugovoj, J. P. Toennies and A. Vilesov, *J. Chem. Phys.*, 2000, **112**, 8217–8220.
- 49 T. Raz and R. D. Levine, *Chem. Phys. Lett.*, 1995, **246**, 405–412.
- 50 J. D. Beckerle, Q. Y. Yang, A. D. Johnson and S. T. Ceyer, *J. Chem. Phys.*, 1987, **86**, 7236–7237.
- 51 T. N. V. Nguyen, Q. K. Timerghazin, H. Vach and G. H. Peslherbe, *J. Chem. Phys.*, 2011, **134**, 064305.
- 52 C. Jouvet and B. Soep, *Chem. Phys. Lett.*, 1983, **96**, 426–428.
- 53 G. Del Mistro and A. J. Stace, *Chem. Phys. Lett.*, 1992, **196**, 67.
- 54 P. de Pujo, J.-M. Mestdagh, J. P. Visticot, J. Cuvellier, P. Meynadier, O. Sublemontier, A. Lallement and J. Berlande, *Z. Phys. D*, 1993, **25**, 357–362.
- 55 M. P. Gaigeot, P. de Pujo, V. Brenner and P. Millié, *J. Chem. Phys.*, 1997, **106**, 9155–9171.
- 56 J. Douady, S. Awali, L. Poisson, B. Soep, J.-M. Mestdagh and B. Gervais, *J. Phys. Chem. A*, 2015, 6074–6081.
- 57 S. Awali, M. A. Gaveau, M. Briant, J. M. Mestdagh, B. Soep, O. Gobert, R. Maksimenka and L. Poisson, *Phys. Chem. Chem. Phys.*, 2016, **18**, 32378–32386.
- 58 A. Masson, L. Poisson, M.-A. Gaveau, B. Soep, J.-M. Mestdagh, V. Mazet and F. Spiegelman, *J. Chem. Phys.*, 2010, **133**, 054307.
- 59 M. Ben El Hadj Rhouma, H. Berriche, Z. B. Lakhdar and F. Spiegelman, *J. Chem. Phys.*, 2002, **116**, 1839–1849.
- 60 J. Liang and V. V. Kresin, *J. Chem. Phys.*, 2020, **153**, 196101.
- 61 S. Awali, J.-M. Mestdagh, M.-A. Gaveau, M. Briant, B. Soep, V. Mazet and L. Poisson, *J. Phys. Chem. A*, 2021, **125**, 4341–4351.
- 62 J. Vigué, P. Labastie and F. Calvo, *Eur. Phys. J. D*, 2000, **8**, 265–272.
- 63 J. Gspann and H. Vollmar, in *Rarefied Gas Dynamics*, ed. K. Karamcheti, Academic Press, New York, 1974, pp. 261–267.
- 64 J. Gspann and H. Vollmar, in *Rarefied Gas Dynamics*, ed. R. Campargue, Commissariat à l’Energie Atomique, Paris, 1978, vol. II, pp. 1193–1205.
- 65 J. Tiggesbaumer and F. Stienkemeier, *Phys. Chem. Chem. Phys.*, 2007, **9**, 4748–4770.

- 66 O. Bunermann and F. Stienkemeier, *Eur. Phys. J. D*, 2011, **61**, 645–655.
- 67 A. Vilà, M. González and R. Mayol, *Phys. Chem. Chem. Phys.*, 2016, **18**, 2006–2014.
- 68 F. Coppens, F. Ancilotto, M. Barranco, N. Halberstadt and M. Pi, *Phys. Chem. Chem. Phys.*, 2017, **19**, 24805–24818.
- 69 M. Blancafort-Jorquera, A. Vilà and M. González, *Phys. Chem. Chem. Phys.*, 2018, **20**, 29737–29753.
- 70 A. Vilà and M. González, *Phys. Chem. Chem. Phys.*, 2016, **18**, 31869–31880.
- 71 M. Blancafort-Jorquera, A. Vilà and M. González, *Phys. Chem. Chem. Phys.*, 2019, **21**, 24218–24231.
- 72 A. Leal, D. Mateo, A. Hernando, M. Pi and M. Barranco, *Phys. Chem. Chem. Phys.*, 2014, **16**, 23206–23213.
- 73 J. Fedor, V. Poterya, A. Pysanenko and M. Fárnik, *J. Chem. Phys.*, 2011, **135**, 104305.
- 74 K. Nauta and R. E. Miller, *Science*, 1999, **283**, 1895–1897.
- 75 K. Nauta and R. E. Miller, *Science*, 2000, **287**, 293–295.
- 76 L. F. Gomez, E. Loginov and A. F. Vilesov, *Phys. Rev. Lett.*, 2012, **108**, 155302.
- 77 O. Gessner and A. F. Vilesov, *Annu. Rev. Phys. Chem.*, 2019, **70**, 173–198.
- 78 B. W. van de Waal, G. Torchet and M. F. de Feraudy, *Chem. Phys. Lett.*, 2000, **331**, 57–63.
- 79 R. S. Berry and B. M. Smirnov, in *Structure and Bonding*, ed. D. M. P. Mingos, Springer, Heidelberg, Dordrecht, London, New York, 2012, vol. 143, pp. 221–230.
- 80 J. Farges, M. F. de Feraudy, R. Raoult and G. Torchet, *J. Chem. Phys.*, 1983, **78**, 5067.
- 81 J. Farges, M. F. de Feraudy, B. Raoult and G. Torchet, *J. Chem. Phys.*, 1986, **84**, 3491.
- 82 G. Torchet, J. Farges, M. F. de Feraudy and B. Raoult, in *The Chemical Physics of Atomic and Molecular Clusters*, ed. G. Scoles, North Holland, Amsterdam, 1990, pp. 513–542.
- 83 L. Perera and F. G. Amar, *J. Chem. Phys.*, 1990, **93**, 4884.
- 84 J. P. Visticot, P. de Pujo, J.-M. Mestdagh, A. Lallement, J. Berlande, O. Sublemontier, P. Meynadier and J. Cuvellier, *J. Chem. Phys.*, 1994, **100**, 158–164.
- 85 F. Calvo, F. Spiegelman and J.-M. Mestdagh, *J. Chem. Phys.*, 2003, **118**, 8763–8769.
- 86 F. Spiegelman, L. Maron, W. H. Breckenridge, J. M. Mestdagh and J. P. Visticot, *J. Chem. Phys.*, 2002, **117**, 7534–7550.
- 87 A. Lallement, O. Sublemontier, J. P. Visticot, A. J. Bell, J. Berlande, J. Cuvellier, J.-M. Mestdagh and P. Meynadier, *Chem. Phys. Lett.*, 1993, **204**, 440–444.
- 88 J.-M. Mestdagh, A. J. Bell, J. Berlande, X. Biquard, M.-A. Gaveau, A. Lallement, O. Sublemontier and J. P. Visticot, in *Reactions Dynamics in Clusters and Condensed Phases*, ed. J. Jortner, R. D. Levine and B. Pullman, Kluwer, Dordrecht, 1994, vol. 26 of The Jerusalem Symposium on Quantum Chemistry and Biochemistry, pp. 101–114.
- 89 M. Briant, M.-A. Gaveau, J.-M. Mestdagh and J. P. Visticot, *J. Chem. Phys.*, 2000, **112**, 1744–1756.
- 90 H. Sano and M. Tachiya, *J. Chem. Phys.*, 1981, **75**, 2870–2878.
- 91 E. H. C. Parker, H. R. Glyde and B. L. Smith, *Phys. Rev.*, 1968, **176**, 1107–1110.
- 92 L. E. Fried and S. Mukamel, *Phys. Rev. Lett.*, 1991, **66**, 2340–2343.
- 93 L. E. Fried and S. Mukamel, *J. Chem. Phys.*, 1992, **96**, 116–135.
- 94 M. Dvorak, M. Müller, T. Knoblauch, O. Bünermann, A. Rydlo, S. Minniberger, W. Harbich and F. Stienkemeier, *J. Chem. Phys.*, 2012, **137**, 164301.
- 95 M. Dvorak, M. Müller, T. Knoblauch, O. Bünermann, A. Rydlo, S. Minniberger, W. Harbich and F. Stienkemeier, *J. Chem. Phys.*, 2012, **137**, 164302.
- 96 J. Stapelfeldt, J. Wörmer and T. Möller, *Phys. Rev. Lett.*, 1989, **62**, 98.
- 97 T. Möller and G. Zimmerer, *J. Opt. Soc. Am. B*, 1989, **6**, 1062–1071.
- 98 J. Stapelfeldt, J. Wörmer, G. Zimmerer and T. Möller, *Zeitschrift für Physik D Atoms, Molecules and Clusters*, 1989, **12**, 435–437.
- 99 M. C. Castex, M. Morlais, F. Spiegelmann and J. P. Malrieu, *J. Chem. Phys.*, 1981, **75**, 5006–5018.
- 100 P. Duplaa and F. Spiegelmann, *J. Chem. Phys.*, 1996, **105**, 1500–1515.
- 101 N. Schwentner, E.-E. Koch and J. Jortner, in *Electronic Excitations in Condensed Rare Gases*, Springer Berlin Heidelberg, Berlin, Heidelberg, 1985, pp. 22–62.
- 102 J. Singh, in *Excitation Energy Transfer Processes in Condensed Matter: Theory and Applications*, ed. J. Singh, Springer US, Boston, MA, 1994, pp. 1–45.
- 103 E. V. Savchenko, G. Zimmerer and V. E. Bondybey, *J. Lumin.*, 2009, **129**, 1866–1868.
- 104 F. Y. Naumkin and D. J. Wales, *Mol. Phys.*, 1999, **96**, 1295–1304.
- 105 A. Lietard, G. Piani, M. Briant, M.-A. Gaveau, S. Faisan, V. Mazet, B. Soep, J.-M. Mestdagh and L. Poisson, *Phys. Chem. Chem. Phys.*, 2018, **20**, 11206–11214.
- 106 A. Eppink and D. H. Parker, *Rev. Sci. Instrum.*, 1997, **68**, 3477–3484.
- 107 C. Vallance, D. Heathcote and J. W. L. Lee, *J. Phys. Chem. A*, 2021, **125**, 1117–1133.
- 108 A. Stolow, A. E. Bragg and D. M. Neumark, *Chem. Rev.*, 2004, **104**, 1719–1757.
- 109 J. R. R. Verlet, A. E. Bragg, A. Kammrath, O. Cheshnovsky and D. M. Neumark, *J. Chem. Phys.*, 2004, **121**, 10015–10025.
- 110 E. S. Peterson, B. J. Schwartz and C. B. Harris, *J. Chem. Phys.*, 1993, **99**, 1693–1702.
- 111 P. Y. Serdobintsev, A. S. Melnikov, A. A. Pastor, N. A. Timofeev and M. A. Khodorkovskiy, *J. Chem. Phys.*, 2018, **148**, 194301.
- 112 F. Vigliotti, L. Bonacina, M. Chergui, G. Rojas-Lorenzo and J. Rubayo-Soneira, *Chem. Phys. Lett.*, 2002, **362**, 31–38.

- 113 F. Vigliotti, L. Bonacina and M. Chergui, *Phys. Rev. B*, 2003, **6711**, 5118–5118.
- 114 G. Rojas-Lorenzo, J. Rubayo-Soneira, F. Vigliotti and M. Chergui, *Phys. Rev. B*, 2003, **6711**, 5119–5119.
- 115 A. Golan and M. Ahmed, *J. Phys. Chem. Lett.*, 2012, **3**, 458–462.
- 116 W. C. Lu, R. B. Metz, T. P. Troy, O. Kostko and M. Ahmed, *Phys. Chem. Chem. Phys.*, 2020, **22**, 14284–14292.
- 117 H. Hotop and A. Niehaus, *Zeitschrift für Physik*, 1968, **215**, 395–407.
- 118 S. Falcinelli, F. Pirani, P. Candori, B. G. Brunetti, J. M. Farrar and F. Vecchiocattivi, *Frontiers in Chemistry*, 2019, **7**, 445.
- 119 F. Calvo, D. Bonhommeau and P. Parneix, *Phys. Rev. Lett.*, 2007, **99**, 083401.
- 120 M. Mudrich and F. Stienkemeier, *Int. Rev. Phys. Chem.*, 2014, **33**, 301–339.
- 121 M. P. Ziemkiewicz, D. M. Neumark and O. Gessner, *Int. Rev. Phys. Chem.*, 2015, **34**, 239–267.
- 122 K. von Haeften, T. Laarmann, H. Wabnitz and T. Möller, *Phys. Rev. Lett.*, 2002, **88**, 233401.
- 123 K. D. Closser, O. Gessner and M. Head-Gordon, *J. Chem. Phys.*, 2014, **140**, 134306.
- 124 R. Karnbach, M. Joppien and T. Möller, *J. Chimie Phys.*, 1995, **92**, 499–520.
- 125 C. C. Wang, O. Kornilov, O. Gessner, J. H. Kim, D. S. Peterka and D. M. Neumark, *J. Phys. Chem. A*, 2008, **112**, 9356–9365.
- 126 M. Shcherbinin, A. C. LaForge, M. Hanif, R. Richter and M. Mudrich, *J. Phys. Chem. A*, 2018, **122**, 1855–1860.
- 127 S. Mandal, R. Gopal, M. Shcherbinin, A. D'Elia, H. Srinivas, R. Richter, M. Coreno, B. Bapat, M. Mudrich, S. R. Krishnan and V. Sharma, *Phys. Chem. Chem. Phys.*, 2020, **22**, 10149–10157.
- 128 C. Callegari, J. Higgins, F. Stienkemeier and G. Scoles, *J. Phys. Chem. A*, 1998, **102**, 95–101.
- 129 J. Reho, J. Higgins, C. Callegari, K. K. Lehmann and G. Scoles, *J. Chem. Phys.*, 2000, **113**, 9686–9693.
- 130 J. Reho, J. Higgins, K. K. Lehmann and G. Scoles, *J. Chem. Phys.*, 2000, **113**, 9694–9701.
- 131 E. Loginov, A. Hernando, J. A. Beswick, N. Halberstadt and M. Drabbels, *J. Phys. Chem. A*, 2015, **119**, 6033–6044.
- 132 C. P. Schulz, P. Claas and F. Stienkemeier, *Phys. Rev. Lett.*, 2001, **8715**, 153401.
- 133 J. von Vangerow, F. Coppens, A. Leal, M. Pi, M. Barranco, N. Halberstadt, F. Stienkemeier and M. Mudrich, *J. Phys. Chem. Lett.*, 2017, **8**, 307–312.
- 134 M. Martinez, F. Coppens, M. Barranco, N. Halberstadt and M. Pi, *Phys. Chem. Chem. Phys.*, 2019, **21**, 3626–3636.
- 135 J.-M. Mestdagh, J. Berlande, P. de Pujo, J. Cuvellier and A. Binet, *Z. Phys. A*, 1982, **304**, 3–10.
- 136 F. Coppens, J. von Vangerow, M. Barranco, N. Halberstadt, F. Stienkemeier, M. Pi and M. Mudrich, *Phys. Chem. Chem. Phys.*, 2018, **20**, 9309–9320.
- 137 N. V. Dozmorov, A. V. Baklanov, J. von Vangerow, F. Stienkemeier, J. A. M. Fordyce and M. Mudrich, *Phys. Rev. A*, 2018, **98**, 043403.
- 138 B. Gervais, D. Zanuttini and J. Douady, *J. Chem. Phys.*, 2016, **144**, 194307.
- 139 S. Awali, L. Poisson, B. Soep, M.-A. Gaveau, M. Briant, C. Pothier, J.-M. Mestdagh, M. Ben El Hadj Rhouma, M. Hochlaf, V. Mazet and S. Faisan, *Phys. Chem. Chem. Phys.*, 2014, **16**, 516–526.
- 140 M.-C. Heitz, L. Teixidor, N. T. Van-Oanh and F. Spiegelman, *J. Phys. Chem. A*, 2010, **114**, 3287–3296.
- 141 A. Masson, M.-C. Heitz, J.-M. Mestdagh, M.-A. Gaveau, L. Poisson and F. Spiegelman, *Phys. Rev. Lett.*, 2014, **113**, 123005.
- 142 I. Janecek, S. Cintavá, D. Hrivňák, K. Kalus, M. Fárník and F. X. Gadea, *J. Chem. Phys.*, 2009, **131**, 114306.
- 143 E. Loginov and M. Drabbels, *Phys. Rev. Lett.*, 2011, **106**, 083401.
- 144 E. Loginov, C. Callegari, F. Ancilotto and M. Drabbels, *J. Phys. Chem. A*, 2011, **115**, 6779–6788.
- 145 F. Lackner, G. Krois, M. Theisen, M. Koch and W. E. Ernst, *Phys. Chem. Chem. Phys.*, 2011, **13**, 18781–18788.
- 146 F. Lackner, G. Krois, M. Koch and W. E. Ernst, *J. Phys. Chem. Lett.*, 2012, **3**, 1404–1408.
- 147 B. Thaler, S. Ranftl, P. Heim, S. Cesnik, L. Treiber, R. Meyer, A. W. Hauser, W. E. Ernst and M. Koch, *Nat. Commun.*, 2018, **9**, 4006.
- 148 L. Andrews and G. C. Pimentel, *J. Chem. Phys.*, 1967, **47**, 2905–2910.
- 149 L. C. Balling, M. D. Havey and J. J. Wright, *J. Chem. Phys.*, 1979, **70**, 2404–2408.
- 150 J. J. Wright and L. C. Balling, *J. Chem. Phys.*, 1980, **73**, 3103–3106.
- 151 C. Crépin and A. Tramer, *Chem. Phys.*, 2001, **272**, 227–241.
- 152 C. Crépin, C. Gée, A. Cuisset, L. Divay, A. Tramer and P. de Pujo, *J. Lumines.*, 2001, **94**, 457–460.
- 153 C. Crépin, P. de Pujo, B. Bouvier, V. Brenner and P. Millie, *Chem. Phys.*, 2001, **272**, 243–258.
- 154 C. Gée, A. Cuisset, L. Divay and C. Crépin, *J. Chem. Phys.*, 2002, **116**, 4993–5001.
- 155 M. Ryan, M. Collier, P. de Pujo, C. Crépin and J. G. McCaffrey, *J. Phys. Chem. A*, 2010, **114**, 3011–3024.
- 156 E. Jacquet, D. Zanuttini, J. Douady, E. Giglio and B. Gervais, *J. Chem. Phys.*, 2011, **135**, 174503.
- 157 R. Thon, W. Chin, J.-P. Galaup, A. Ouvrard, B. Bourguignon and C. Crépin, *J. Phys. Chem. A*, 2013, **117**, 8145–8156.
- 158 R. Thon, W. Chin, D. Chamma, A. Gutiérrez-Quintanilla, M. Chevalier, J.-P. Galaup and C. Crépin, *J. Lumin.*, 2017, **191**, 78–86.
- 159 S. Arabei, J. G. McCaffrey, J.-P. Galaup, N. Shafizadeh and C. Crépin, *Phys. Chem. Chem. Phys.*, 2015, **17**, 14931–14942.
- 160 D. H. Parker and P. Avouris, *Chem. Phys. Lett.*, 1978, **53**, 515–520.
- 161 D. H. Parker and P. Avouris, *J. Chem. Phys.*, 1979, **71**, 1241–

- 1246.
- 162 D. Consalvo, J. Oomens, D. H. Parker and J. Reuss, *Chem. Phys.*, 1992, **163**, 223–239.
- 163 L. Poisson, R. Maksimenska, B. Soep, J.-M. Mestdagh, D. H. Parker, M. Nsangou and M. Hochlaf, *J. Phys. Chem. A*, 2010, **114**, 3313–3319.
- 164 K. Mathivon, R. Linguerrri and M. Hochlaf, *J. Chem. Phys.*, 2013, **139**, 164306.
- 165 K. Mathivon, R. Linguerrri and M. Hochlaf, *J. Mol. Model.*, 2014, **20**, 2135.
- 166 Q. Y. Shang and E. R. Bernstein, *Chem. Rev.*, 1994, **94**, 2015–2025.
- 167 P. F. Bernath, *Spectra of Atoms and Molecules*, 2nd ed, Oxford University Press, N.Y., 2005.
- 168 A. M. Halpern and R. M. Danziger, *Chem. Phys. Lett.*, 1972, **16**, 72–76.
- 169 A. Lietard, G. Gallician, J. Tan, M. A. Gaveau, M. Briant, B. Soep, J. M. Mestdagh and L. Poisson, *Mol. Phys.*, 2021, **119**, e1737743.
- 170 J. S. Baskin and A. H. Zewail, *J. Phys. Chem.*, 1994, **98**, 3337–3351.
- 171 A. Lietard, G. Piani, R. Pollet, B. Soep, L. Poisson and J. M. Mestdagh, *Phys. Chem. Chem. Phys.*, Submitted.
- 172 D. R. Herschbach, *Chemica Scripta*, 1987, **27**, 327–347.
- 173 Y. T. Lee, *Science*, 1987, **236**, 793.
- 174 J. C. Polanyi, *Chemica Scripta*, 1987, **27**, 229–247.
- 175 B. Soep, C. J. Whitham, A. Keller and J. P. Visticot, *Faraday Discuss.*, 1991, **91**, 191–205.
- 176 B. Soep, S. Abbes, A. Keller and J. P. Visticot, *J. Chem. Phys.*, 1992, **96**, 440–449.
- 177 A. Keller, R. Lawruszczuk, B. Soep and J. P. Visticot, *J. Chem. Phys.*, 1996, **105**, 4556–4564.
- 178 M. Briant, P. R. Fournier, M.-A. Gaveau, J.-M. Mestdagh, B. Soep and J. P. Visticot, *J. Chem. Phys.*, 2002, **117**, 5036–5047.
- 179 P. Piecuch, *J. Mol. Struct.*, 1997, **436-437**, 503–536.
- 180 J.-M. Mestdagh, F. Spiegelman, E. Gloaguen, M. Collier, F. Lepetit, M.-A. Gaveau, C. S. Sanz and B. Soep, *J. Phys. Chem. A*, 2006, **110**, 7355–7363.
- 181 E. Gloaguen, C. Sanz Sanz, M. Collier, M.-A. Gaveau, B. Soep, O. Roncero and J.-M. Mestdagh, *J. Phys. Chem. A*, 2008, **112**, 1408–1420.
- 182 M. Briant, E. Gloaguen, A. Beswick, J.-M. Mestdagh, S. Stolte, L. Poisson, C. Pothier and B. Soep, *J. Phys. Chem. A*, 2015, 6099–6110.
- 183 M.-A. Gaveau, E. Gloaguen, P. R. Fournier and J. M. Mestdagh, *J. Phys. Chem. A*, 2005, **109**, 9494–9498.
- 184 D. Verma, R. M. P. Tanyag, S. M. O. O’Connell and A. F. Vilesov, *Advances in Physics: X*, 2019, **4**, 1553569.
- 185 Y. Kwon, P. Huang, M. V. Patel, D. Blume and K. B. Whaley, *J. Chem. Phys.*, 2000, **113**, 6469–6501.
- 186 M. Lemeshko, *Phys. Rev. Lett.*, 2017, **118**, 095301.
- 187 M. Briant, E. Mengesha, P. de Pujo, M.-A. Gaveau, B. Soep, J.-M. Mestdagh and L. Poisson, *Phys. Chem. Chem. Phys.*, 2016, **18**, 16414–16422.
- 188 M. Briant, A. Viel, E. Mengesha, M.-A. Gaveau, B. Soep, J.-M. Mestdagh, P. Jamet, J.-M. Launay and L. Poisson, *Phys. Chem. Chem. Phys.*, 2019, **21**, 1038–1045.
- 189 M. Briant, E. Mengesha, M. A. Gaveau, B. Soep, J. M. Mestdagh and L. Poisson, *Phys. Chem. Chem. Phys.*, 2018, **20**, 2597–2605.
- 190 C. Callegari, K. K. Lehmann, R. Schmied and G. Scoles, *J. Chem. Phys.*, 2001, **115**, 10090–10110.
- 191 G. Guillon, A. Viel and J. Launay, *J. Chem. Phys.*, 2012, **136**, 174307–1–7.
- 192 A. Viel and J. Launay, *J. Phys. Chem. A*, 2014, **118**, 6529–6535.
- 193 A. Simoni, A. Viel and J. Launay, *J. Chem. Phys.*, 2017, **146**, 244106.
- 194 C. Lauzin, E. Cauet, J. Demaison, M. Herman, H. Stoll and J. Liévin, *Mol. Phys.*, 2012, **110**, 2751–2760.
- 195 C. Lauzin, L. H. Coudert, M. Herman and J. Liévin, *J. Phys. Chem. A*, 2013, **117**, 13767–13774.
- 196 R. J. Bemish, P. A. Block, L. G. Pedersen, W. T. Yang and R. E. Miller, *J. Chem. Phys.*, 1993, **99**, 8585–8598.
- 197 J. M. Hutson, in *Advances in Molecular Vibrations and Collision Dynamics*, ed. J. M. Bowman, JAI Press, 1991, vol. 1, pp. 1–46.
- 198 K. Nauta and R. E. Miller, *J. Chem. Phys.*, 2001, **115**, 8384–8392.
- 199 R. E. Zillich, Y. Kwon and K. B. Whaley, *Phys. Rev. Lett.*, 2004, **93**, 250401.
- 200 A. Vilà, M. González and R. Mayol, *J. Chem. Theory Comput.*, 2015, **11**, 899–906.
- 201 A. Vilà, M. Paniagua and M. González, *Phys. Chem. Chem. Phys.*, 2018, **20**, 118–130.
- 202 M. Blancafort-Jorquera, A. Vilà and M. González, *Phys. Chem. Chem. Phys.*, 2019, **21**, 21007–21021.
- 203 R. J. Donovan, D. Husain and L. J. Kirsch, *Annual Reports on the Progress of Chemistry, Section A: General Physical and Inorganic Chemistry*, 1972, **69**, 19–74.
- 204 J. M. C. Plane, in *Gas Phase Metal Reactions*, ed. A. Fontijn, Elsevier, Amsterdam, 1992, pp. 29–56.
- 205 R. A. Perry and J. A. Miller, *International Journal of Chemical Kinetics*, 1996, **28**, 217–234.
- 206 B. Gao, J.-x. Zhao, Q.-h. Cai, X.-g. Wang and X.-z. Wang, *J. Phys. Chem. A*, 2011, **115**, 9969–9976.
- 207 E. S. Kryachko, C. Vinckier and M. T. Nguyen, *J. Chem. Phys.*, 2001, **114**, 7911–7917.
- 208 J. M. C. Plane and C. F. Nien, *J. Phys. Chem.*, 1990, **94**, 5255–5261.
- 209 C. Vinckier, J. Helaers and J. Remeysen, *J. Phys. Chem. A*, 1999, **103**, 5328–5335.
- 210 O. Tishchenko, C. Vinckier, A. Ceulemans and M. T. Nguyen, *J. Phys. Chem. A*, 2005, **109**, 6099–6103.
- 211 C. Ottinger and R. N. Zare, *Chem. Phys. Lett.*, 1970, **5**, 243.
- 212 C. D. Jonah, R. N. Zare and C. Ottinger, *J. Chem. Phys.*, 1972,

- 56, 263–+.
- 213 P. J. Dagdigian, *Chem. Phys. Lett.*, 1978, **55**, 239–244.
- 214 J. A. Irvin and P. J. Dagdigian, *J. Chem. Phys.*, 1981, **74**, 6178–6187.
- 215 R. W. Field, G. A. Capelle and C. R. Jones, *J. Mol. Spectrosc.*, 1975, **54**, 156–159.
- 216 R. F. Marks, R. A. Gottscho and R. W. Field, *Phys. Scr.*, 1982, **25**, 312–328.
- 217 R. F. Marks, H. S. Schweda, R. A. Gottscho and R. W. Field, *J. Chem. Phys.*, 1982, **76**, 4689–4691.
- 218 R. F. Marks, H. S. Schweda, R. A. Gottscho and R. W. Field, *J. Chem. Phys.*, 1982, **77**, 4795–4795.
- 219 C. S. Wei, S. W. Guo and Y. P. Lee, *J. Chem. Phys.*, 1985, **82**, 2942–2946.
- 220 C. Focsa, A. Poclet, B. Pinchemel, R. J. Le Roy and P. F. Bernath, *J. Mol. Spectrosc.*, 2000, **203**, 330–338.
- 221 A. v. Groenendael, M. Tudorie, C. Focsa, B. Pinchemel and P. F. Bernath, *J. Mol. Spectrosc.*, 2005, **234**, 255–263.
- 222 H. Khalil, V. Brites, F. Le Quéré and C. Léonard, *Chem. Phys.*, 2011, **386**, 50–55.
- 223 H. Khalil, F. Le Quéré, V. Brites and C. Léonard, *J. Mol. Spectrosc.*, 2012, **271**, 1–9.
- 224 J. X. Cheng, H. J. Chen, X. J. Zhu and X. L. Cheng, *J. Mol. Struct.*, 2015, **1084**, 122–127.
- 225 C. Gée, M.-A. Gaveau, J.-M. Mestdagh, M. Osborne, O. Sublemontier and J. P. Visticot, *J. Phys. Chem.*, 1996, **100**, 13421 – 13427.
- 226 M.-A. Gaveau and P. R. Fournier, in *XXVth International Symposium on Rarefied Gas Dynamics*, ed. M. S. Ivanov and A. K. Rebrov, Russian Academy of Sciences, Siberian Branch, St Petersburg, Russia, 2007, pp. 1288–1295.
- 227 G. A. Capelle, C. R. Jones, J. Zorskie and H. P. Broida, *J. Chem. Phys.*, 1974, **61**, 4777–4779.
- 228 M.-A. Gaveau, M. Briant, V. Vallet, J.-M. Mestdagh and J. P. Visticot, in *Atomic and Molecular Beams, The State of the Art*, ed. R. Campargue, Springer-Verlag, Berlin, 2001, ch. VI, pp. 827–838.
- 229 M.-A. Gaveau, M. Briant and J.-M. Mestdagh, *AIP Conf. Proc.*, 2012, **1501**, 1373–1382.
- 230 J. Sugar and C. Corliss, *J. Phys. Chem. Ref. Data*, 1979, **8**, 865–916.
- 231 D. P. Baldwin and R. W. Field, *J. Mol. Spectrosc.*, 1990, **139**, 77–83.
- 232 J. B. Norman, K. J. Cross, H. S. Schweda, M. Polak and R. W. Field, *Mol. Phys.*, 1989, **66**, 235–268.
- 233 D. P. Baldwin and R. W. Field, *J. Mol. Spectrosc.*, 1989, **133**, 90–95.
- 234 W. J. Balfour and R. F. Whitlock, *Can. J. Phys.*, 1975, **53**, 472–485.
- 235 D. P. Baldwin, E. J. Hill and R. W. Field, *J. Am. Chem. Soc.*, 1990, **112**, 9156–9161.
- 236 W. M. Haynes, *CRC Handbook of Chemistry and Physics*, CRC Press, Boca Raton, Florida, 2012.
- 237 T. J. Lee, A. P. Rendell and P. R. Taylor, *Theoretica Chimica Acta*, 1992, **83**, 165–175.
- 238 P. M. Futerko and A. Fontijn, *J. Chem. Phys.*, 1991, **95**, 8065–8072.
- 239 S. L. Broadley and J. M. C. Plane, *Phys. Chem. Chem. Phys.*, 2010, **12**, 9094–9106.
- 240 D. J. Wales and J. P. K. Doye, *J. Phys. Chem. A*, 1997, **101**, 5111–5116.
- 241 R. L. Johnston, *Dalton Trans.*, 2003, 4193–4207.
- 242 J. M. C. Marques and F. B. Pereira, *Chem. Phys. Lett.*, 2010, **485**, 211–216.
- 243 J. M. Dieterich and B. Hartke, *Mol. Phys.*, 2010, **108**, 279–291.